Numerical Analysis into the Improvement Performance of Ducted Propeller by using Fins: Case Studies on Types B4-70 and Ka4-70

Berlian Arswendo Adietya[1,2], Husein Syahab[1], Mochammad Nasir[3], Wasis Dwi Aryawan[1], I Ketut Aria Pria Utama[1,*]

1 Department of Naval Architecture, Institut Teknologi Sepuluh Nopember,Surabaya, 60111, Indonesia
2 Department of Naval Architecture, Universitas Dipenogoro, Semarang, 50275, Indonesia
3 National Research and Innovation Agency (BRIN), Indonesia

ARTICLE INFO	ABSTRACT
              	Numerical analysis was conducted to assess the impact of fins on the B4-70 and Ka4-70 propeller performance. The study explored different fin variations, specifically bare fins, Propeller Boss Cap Fins (PBCF), and propeller nozzles, using computational fluid dynamics (CFD) simulations. To obtain the best results, the researchers utilized the explicit algebraic stress model (EASM) based on Reynolds-Averaged Navier-Stokes (RANS) equations and turbulence modelling. The primary goal of this study was to improve the energy efficiency of ships by examining various propeller configurations, both open and ducted. The overall conclusions indicated that the B4-70 PBCF convergent and Ka4-70 PBCF divergent with the addition of nozzle 19A exhibited the highest efficiency based on the EASM analysis. The CFD simulation results for both B4-70 and Ka4-70 propellers, utilizing a nozzle 19A with added boss cap fins, revealed several noteworthy phenomena. Firstly, for the B4-70 propeller, efficiency (η_0) at J = 0.6 to J = 0.8 showed an increase of 1% to 2%. Secondly, concerning the Ka4-70 propeller, efficiency (η_0) at J = 0.6 to J = 0.8 increased by 2% to 10%. These findings clearly demonstrate that the use of an ESD, such as the nozzle 19A with added boss cap fins, enhances the propulsion performance of the ship. It is evident that the CFD approach remains suitable and reliable for overall simulations.

1. Introduction

The marine industry recognizes the pressing need for energy conservation and emissions reduction. However, current energy-saving devices (ESDs) primarily target large ocean-going vessels used in global trade, which are indeed more fuel-efficient than other transportation modes on a per-goods-moved basis [1]. Nevertheless, the shipping sector's vital role in the global economy comes at the environmental cost of substantial CO_2 emissions, accounting for approximately 2.89% of anthropogenic CO_2 emissions in 2018 [2]. Countries like Japan, Canada, and the European Union (EU) have set ambitious emissions reduction goals [3]. The International Maritime Organization (IMO) has proposed various solutions to curb greenhouse gas emissions, including improving ship efficiency,

*Corresponding author.
E-mail address: kutama@na.its.ac.id (I Ketut Aria Pria Utama)*

optimizing operations, and transitioning to alternative fuels [4]. The Fourth IMO GHG Study in 2020 highlighted several energy-efficient options for the shipping industry, with Energy Saving Devices (ESDs) being a key focus [5]. Among these, Propeller Boss Cap Fins (PBCF) have gained popularity for their ability to enhance propeller efficiency through reduced hub vortex and torque optimization [6-8].

Integrating an Electrostatic Discharge (ESD) system into a Ducted Propeller configuration holds potential for boosting thrust, while PBCFs can enhance propeller efficiency. These enhancements are particularly advantageous for commercial vessels and traditional fishing boats, impacting the dynamics of fishing gear [9], as well as catamaran-style fishing vessels [10]. These technologies also find applications in submarines, where quiet thrust generation is crucial [11], and niche sectors like glass-bottom tourism boats [12]. Studies on duct systems, including Pre-Duct effects on Ship Propeller-Hull dynamics, have shown improved hull efficiency but potential reductions in open water propeller efficiency [13]. Thus, a holistic approach is essential when designing propulsion systems for diverse aquatic applications.

Implementing these solutions, especially for retrofitting existing vessels, can be challenging due to the required hull, rudder, or stator fin modifications [14-16]. Alternatively, Energy Saving Devices (ESDs) like PBCF offer a means of meeting Energy Efficiency Operation Index (EEOI) requirements with minimal hull alterations. PBCF, consisting of fins attached to the hub boss cap, can be easily installed by replacing the hubcap. Previous Computational Fluid Dynamics (CFD) studies have shown that open propellers, like the B-Series, perform well with PBCF, while the Kaplan series pairs better with ducted configurations [8]. In this study, CFD analysis considered turbulent parameters [17], flow rate influence [18], and the hydrodynamic performance of propellers with a focus on the combination of PBCF and ducted propellers.

To enhance prediction accuracy and overcome turbulence modeling limitations, an explicit algebraic stress model (EASM) was employed. EASM differs from past turbulence models by aiming for better predictions rather than just avoiding turbulence modeling singularity [19]. It calculates the Reynolds stress explicitly, incorporating a nonlinear Reynolds stress term. EASM, while efficient, also addresses issues with the linear eddy-viscosity model, captures anisotropy in Reynolds stress, avoids numerical singularities, and improves model stability and CPU usage compared to the Reynolds Stress Turbulence Model (RSTM) [20]. However, it slightly underestimates viscous resistance, both with and without energy-saving devices, and predicts slightly lower longitudinal vorticity compared to observed values [21].

The novelty in this research paper lies in the addition of the B4-70 and Ka4-70 propellers along with the nozzle 19A, which falls under the category of an accelerating duct, and fins from the Sobol design number 30. These additions have been proven to increase propeller efficiency by 1.3%. Various boss cap types, including default, straight, convergent, and divergent, were also investigated. Additionally, the study employed a Computational Fluid Dynamics (CFD) approach using Reynolds Averaged Navier Stokes Equations (RANSE) with an explicit algebraic stress model (EASM), which has advantages over the k-ε turbulence model. In previous Adietya *et al.,* [22] 2023 research, it only considered either the B4-70 or Ka4-70 propeller along with one of the boss cap types: default, straight, convergent, or divergent. However, in Adietya *et al.,* [8] 2022 study, both the B4-70 and Ka4-70 propellers with an Ae/Ao of 0.55 were examined using the k-ε turbulence model and a Shushkin nozzle B type. The research conducted on the B4-70 and Ka4-70 propellers revealed differences in pressure, velocity, and efficiency for each combination of boss cap types and fins from the Sobol design number 30 when used in conjunction with the nozzle 19A.

2. Methodology

CFD simulations are employed to assess how well a propeller performs, with performance quantified through metrics like thrust (K_T) and torque (K_Q) coefficients as well as efficiency (η_0).

2.1 Modelling

The key specifications of the miniature propeller model are detailed in Table 1, and the propeller types utilized are indicated as B4-70 and Ka4-70. An interesting result emerged from the application of the Sobol design methodology for fin selection, size concluded in Table 2 [23]. This method revealed a significant 1.3% improvement in overall energy efficiency, suggesting its potential as a standard for integrating boss cap fins to enhance the efficiency of the B4-70 propeller.

Table 1
Particular dimension of propeller [24]

Type	Unit	B4-70 and Ka4-70
The number of blades	-	4
Diameter	mm	300
Expanded blade ratio (Ae/Ao)	-	0.7
Pitch diameter ratio		1.2
Angular velocity	rpm	489

Table 2
Sample of Sobol design number 30 [23]

Fin height	Fin length	Pitch	Start angle
0.08 m	0.64 m	28.1°	33.3°

The Following are variations of the B4-70 and Ka4-70 propeller models, starting Figure 1 to 3

(a)   (b)
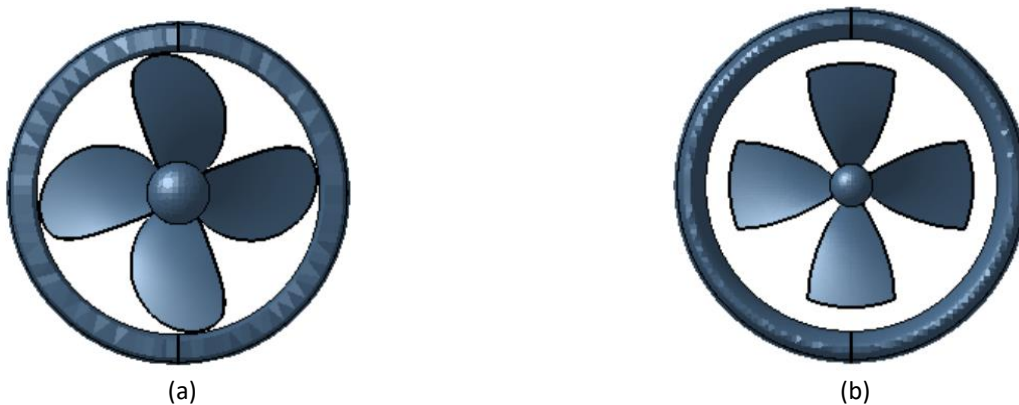**Fig. 1.** Type of propeller (a) Propeller B4-70 nozzle 19A, (b) Propeller B4-70 nozzle 19A

An added level of intricacy is introduced when nozzles are incorporated. In this configuration, known as the nozzle type, the propeller models B4-70 and Ka4-70 are fitted with nozzle 19A. Analyzing this setup offers valuable insights into how the presence of nozzles can influence parameters like K_T, $10K_Q$, and η_0. Figure 1 illustrates the models with nozzle installations, excluding PBCF.
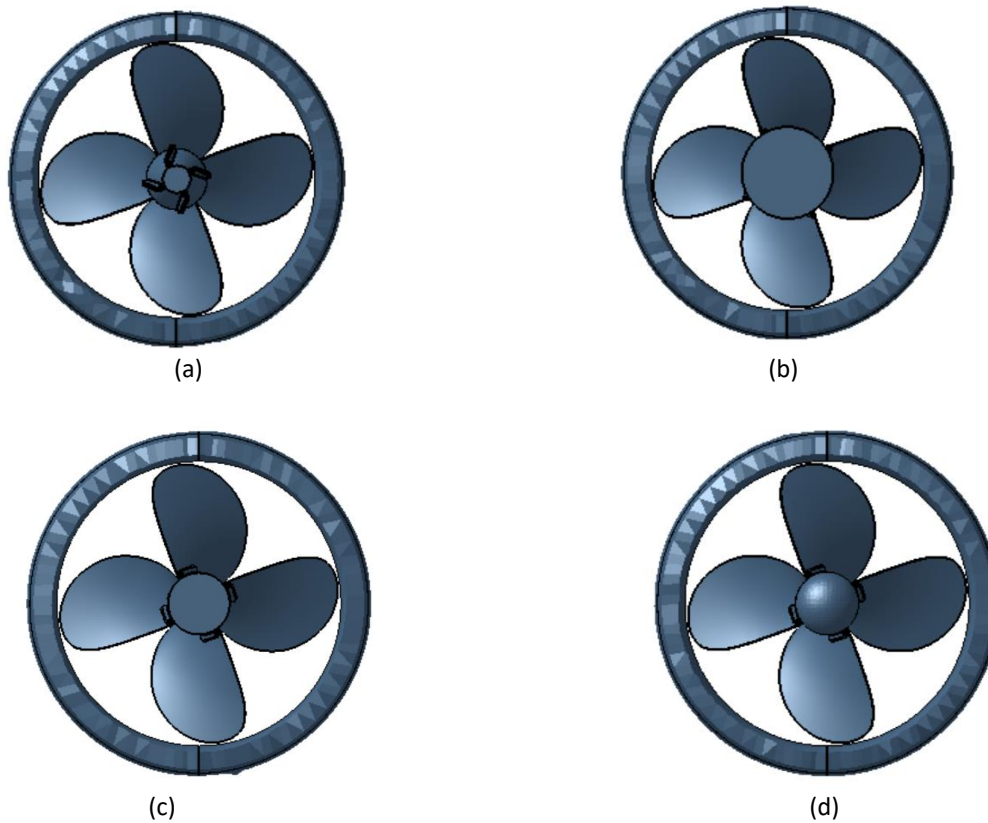
Fig. 2. Type of propeller (a) Propeller B4-70 nozzle and PBCF convergent (b) Propeller B4-70 nozzle and PBCF divergent (c) Propeller B4-70 nozzle and PBCF straight (d) Propeller B4-70 nozzle and PBCF default

The inclusion of nozzles adds an extra level of complexity. In this particular setup, known as the nozzle type, the B4-70 propeller models are fitted with nozzle 19A. Examining this variation offers valuable insights into how the interplay between boss cap fins and nozzles can affect parameters such as K_T, $10K_Q$, and overall η_0. Refer to Figure 2 for an illustration of Propeller B4-70 with PBCF in this context.

An additional layer of intricacy is introduced with the installation of nozzles. In this variation, referred to as the nozzle type, the propeller models Ka4-70 are equipped with nozzle 19A. Evaluating this variation provides insights into how the interaction of boss cap fins and nozzles can impact parameters K_T, $10K_Q$, and its η_0. Figure 3 illustrates the Ka4-70 propeller, which is also equipped with PBCF in this context.
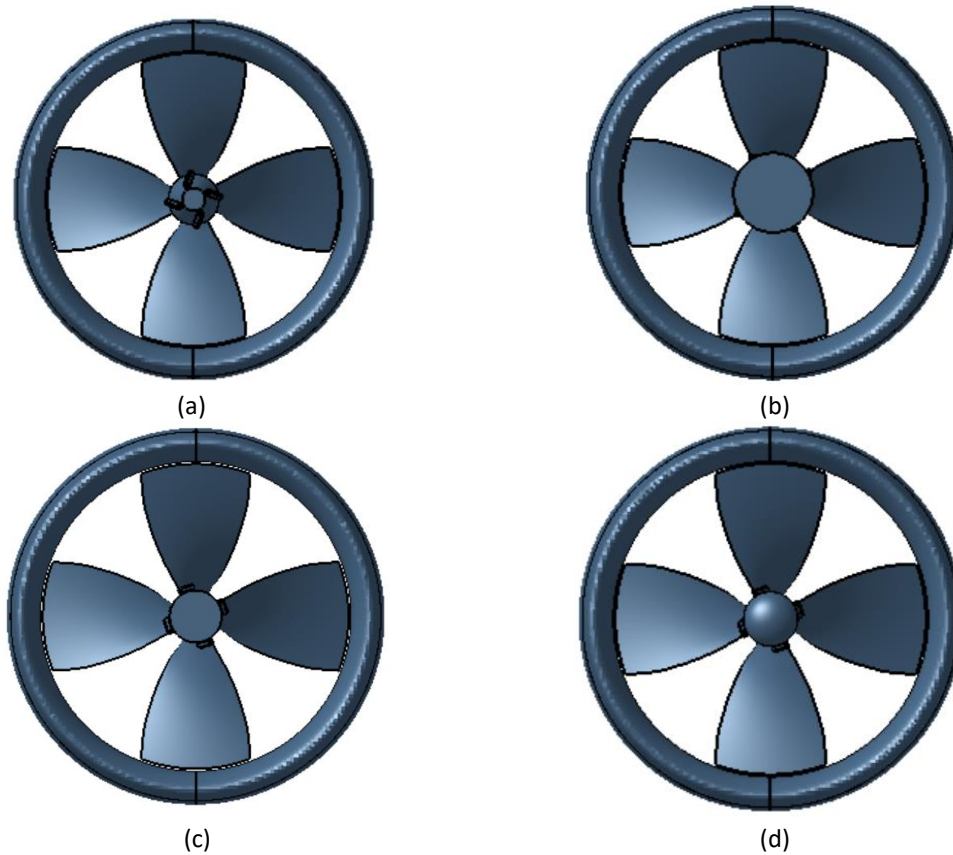
Fig. 3. Type of propeller (a) Propeller Ka4-70 nozzle PBCF convergent (b) Propeller Ka4-70 nozzle PBCF divergent (c) Propeller Ka4-70 nozzle PBCF straight (d) Propeller Ka4-70 nozzle PBCF default

2.2 Numerical Simulation

Numerical simulations are employed to address turbulent phenomena by utilizing the continuity equation, the Reynolds-Averaged Navier-Stokes Equation (RANSE), and the Explicit Algebraic Stress Model (EASM) for turbulence modelling [25]. Eq. (1) and Eq. (2) represent these components:

$$\frac{\partial U_i}{\partial X_i} = 0 \tag{1}$$

Where: ρ is fluid density, *t* is time, U_j is the flow velocity vector field.

$$\frac{\partial U_i}{\partial t} + U_j \frac{\partial U_j}{\partial X_j} = \frac{\partial p}{\partial X_i} + \frac{\partial}{\partial X_j}\left[Re_{eff}^{-1}\left(\frac{\partial U_i}{\partial X_j} + \frac{\partial U_j}{\partial X_i}\right)\right] + S_i \tag{2}$$

Here, Ui stands for Reynolds average velocity components (u, v, w), and xi denotes independent coordinate directions (x, y, z). Si represents the mean strain-rate tensor, while p signifies piezometric pressure, and Reeff denotes effective Reynolds numbers.

For single-point closures, the Reynolds Stress Transport Model (RSTM) is recognized as providing the most accurate depiction of flow physics. However, simplifying the tensor basis involves significant mathematical complexity. Initially, many Explicit Algebraic Stress Models (EASM) are formulated using a 10-term basis, as shown in Eq. (3):

$$b_{ij} = \sum_{\lambda=1}^{10} G^{(\lambda)} T_{ij}^{(\lambda)} \qquad (3)$$

2.3 Boundary Condition

The research defines the boundary conditions for the propellers, as depicted in Figure 4. In the Solid Model, the boundary condition is established as " no-slip". The inlet boundary condition is considered as the "far field." At the outlet boundary, a "Specified Pressure" boundary condition is utilized. Far Field position are extended to the cylindrical surface, ensuring that the entire domain becomes the rotating domain. The size of the rotating frame is designed to be sufficiently large to prevent the Far Field positon from interfering with the simulation of the flow around the propeller.
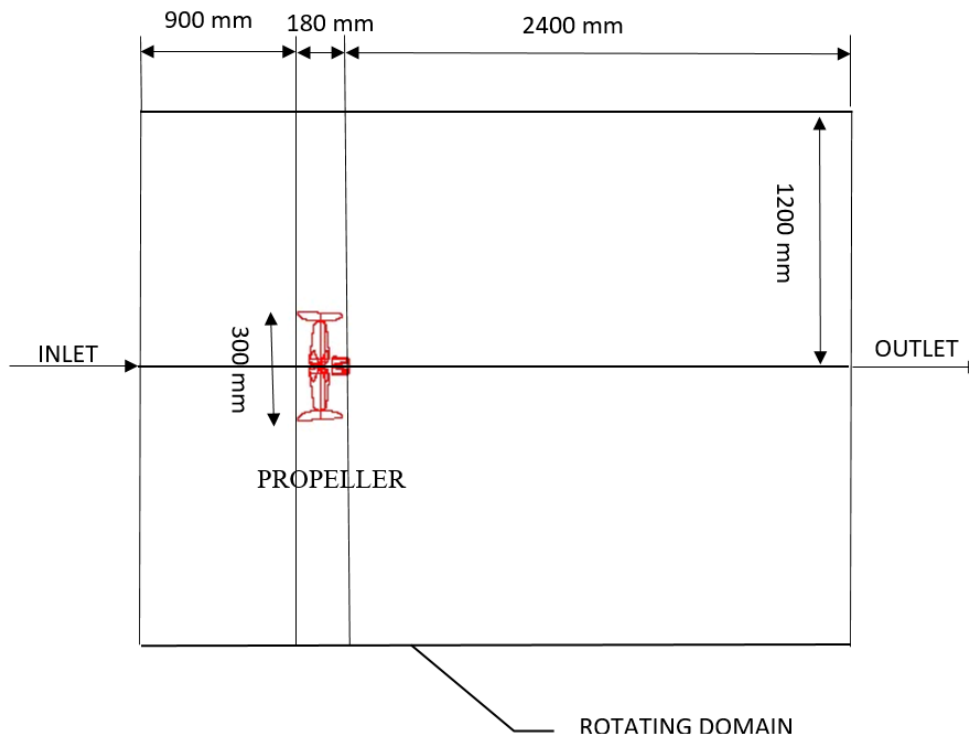

Fig. 4. Boundary condition

Figure 4 illustrates the boundary conditions for the B4-70 and Ka4-70 propellers in this research. The Solid Model defines the boundary condition as "no-slip" The inlet boundary condition is considered to represent the far field (not near field) and a specified pressure is applied as the boundary condition at the outlet. To ensure the entire domain is within the rotating frame, Far Field position are extended to the cylindrical surface. It is essential for the rotating frame to be sufficiently large so that the Far Field position does not interfere with the flow simulation around the propeller. Additionally, the desired domain is a cylinder with a length of 11D and a diameter of 8D, aligned with the symmetry axis of the propeller. The inlet is positioned 3D away from the model, and the outlet is situated 8D away from the model.

2.4 Grid Generation and Grid Independence Test

CFD design was employed to create the mesh structure, as depicted in Figure 5. To ensure the reliability of the simulations, a finer mesh was utilized [25]. Consequently, it is crucial to conduct a

grid independence study. The choice of the mesh density should also be balanced with the computational time, aiming for efficiency and optimization [26]. Moreover, the selection of mesh type and its arrangement significantly impacts the outcomes of the simulations. Opting for the right mesh order has been demonstrated to yield improved results in CFD simulations. Enhancing simulation accuracy involves employing a finer grid around the model interacting with the fluid, which captures interaction phenomena more accurately. Conversely, the distant parts of the fluid can be assigned larger grid sizes to expedite the simulation process. This configuration enhances both computational efficiency and result accuracy.
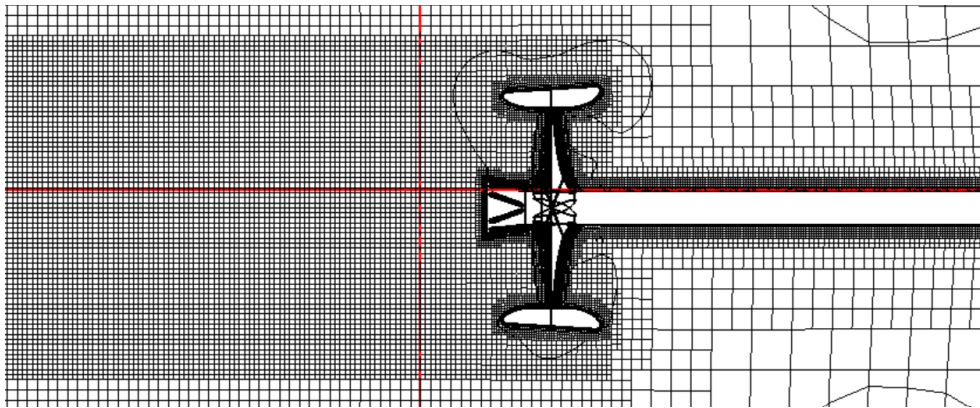

Fig. 5. Meshing of propeller model Ka4-70 with nozzle 19A and PBCF divergent

Additionally, independence grids were incorporated into various components to achieve a consistent number that would result in reduced errors, illustrated in Figure 6. A comparison between numerical and experimental data revealed that the error rate is below 2% [27]. Nevertheless, Table 3 indicates a preference for a value below 1%.
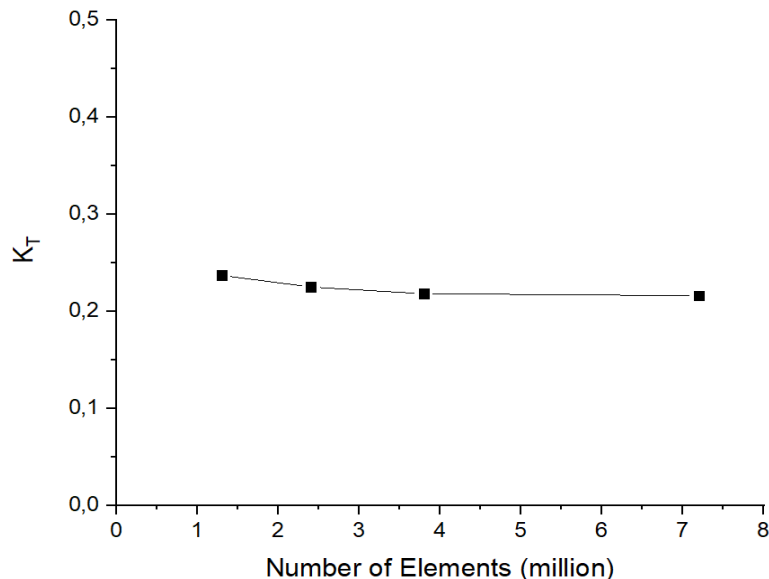

Fig. 6. Grid independence propeller Ka4-70 with nozzle 19A and PBCF for K_T

Table 3
Grid independence propeller Ka4-70 with nozzle 19A and PBCF

Number of elements	1,258,299	2,344,576	3,835,380	7,190,246
K_T	0.237	0.225	0.218	0.216
Percentage	-	1.3%	0.7%	0.2%

2.5 Propeller Efficiency

Propellers are typically positioned on the stern of a vessel to function effectively in various water conditions encountered during navigation. The ship's design and characteristics can significantly influence how the propeller performs. Consequently, it is crucial to assess the fundamental performance attributes of the propeller in open water, independently of the specific vessel. The performance characteristics of a propeller typically encompass changes in thrust, torque, and efficiency as the propeller operates at different speeds and rotational rates in an open water environment. To evaluate these characteristics in open water, experiments are carried out using model propellers towed within a towing tank. During these experiments, variations in the rotation rate and towing velocity are applied to measure the propeller's thrust and torque. The obtained data is then utilized to compute non-dimensional parameters, including the thrust coefficient (K_T), torque coefficient (K_Q), and open water efficiency (η_0). These parameters are graphed against the advance coefficient (J). Eq. (4) to Eq. (7) are used to formulate how to calculate, K_T, K_Q, and η_0.

$$J = \frac{V_A}{nD} \tag{4}$$

$$K_T = \frac{T}{\rho n^2 D^4} \tag{5}$$

$$K_Q = \frac{Q}{\rho n^2 D^5} \tag{6}$$

$$\eta_0 = \frac{v_a}{2\pi nD} \frac{K_T}{K_Q} \tag{7}$$

3. Propeller B4-70 and Ka4-70 with Nozzle
3.1 Propeller B4-70 with Nozzle 19A

The results of propeller B4-70 with nozzle calculation are shown in Figure 7.

The open water test graph of the B4-70 propeller with nozzle 19A, derived from CFD simulations, indicates that the efficiency is minimal at low speeds, while the values of K_T and $10K_Q$ are elevated. As depicted in Figure 7, the propeller demonstrates a declining pattern in K_T and $10K_Q$ with the rise of the advance coefficient (J). In contrast, the efficiency (η_0) shows a converse trajectory, with its lowest point occurring at J = 0.1 and peaking at 0.555 when J = 0.8. In summary, the B4-70 propeller in the configuration with nozzle 19A attains its highest efficiency at J = 0.8, while showcasing elevated K_T and $10K_Q$ values during low speeds. These conclusions are based on the provided simulation data, along with the specific propeller and nozzle 19A setup [28].

The pressure visualization of the B4-70 propeller with nozzle 19A reinforces the results of the CFD simulation in Figure 8. The outcomes presented in the graphs demonstrate that at low speeds, J = 0, there is a high K_T value of 0.324; at moderate speeds, J = 0.5, the K_T value is 0.246; while at high speeds, J = 1.0, the K_T value is 0.114. In the region of the boss cap fins, significant pressure occurs at J = 0.1, exceeding 1000 Pa; similarly, at J = 0.5, the pressure is also above 1000 Pa, but the pressure value is lower at J = 0.5, ranging from 250 to 500 Pa. This study highlights that the B4-70 open

propeller experiences substantial pressure at low speeds, J = 0.1, up to moderate speeds, J = 0.5, indicating a need for a solution to reduce the pressure.

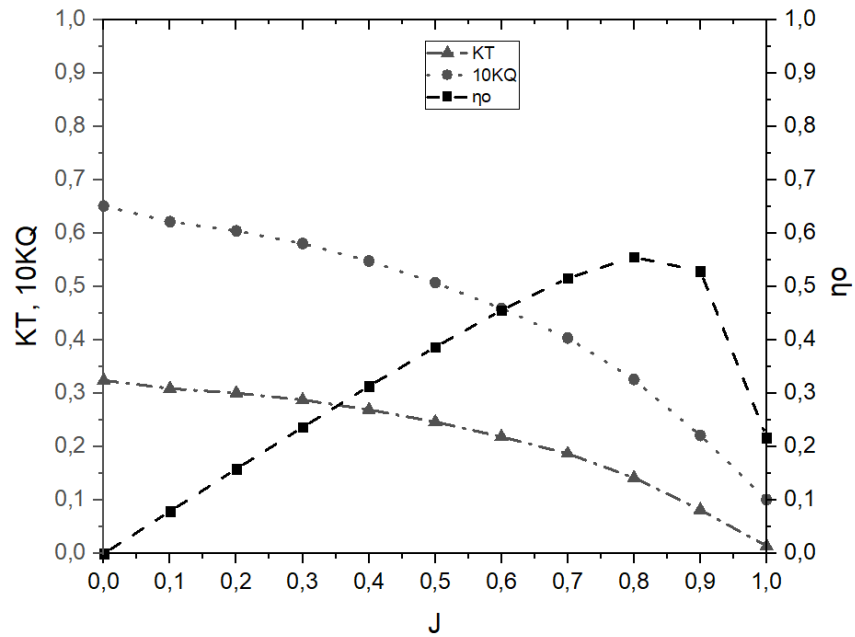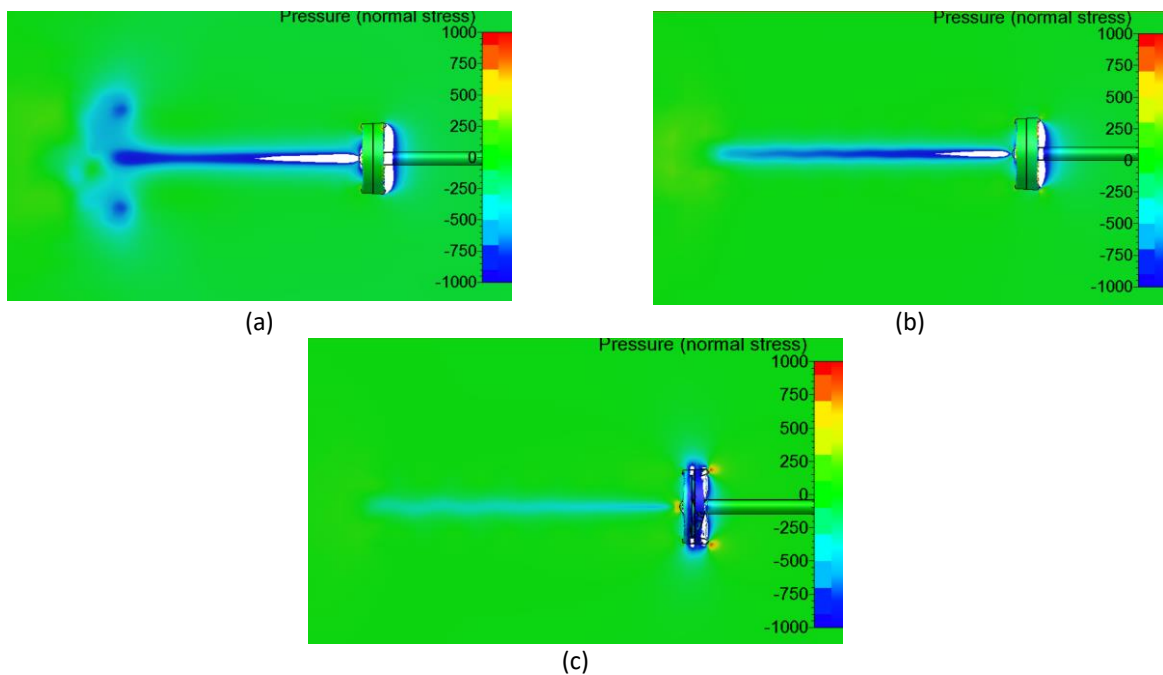**Fig. 7.** Open water test diagram of B4-70 with nozzle 19A

(a)

(b)

(c)

Fig. 8. Visualization of pressure on the B4-70 propeller with nozzle 19A (a) Pressure at J= 0.1 (b) Pressure at J= 0.5 (c) Pressure at J= 0.8
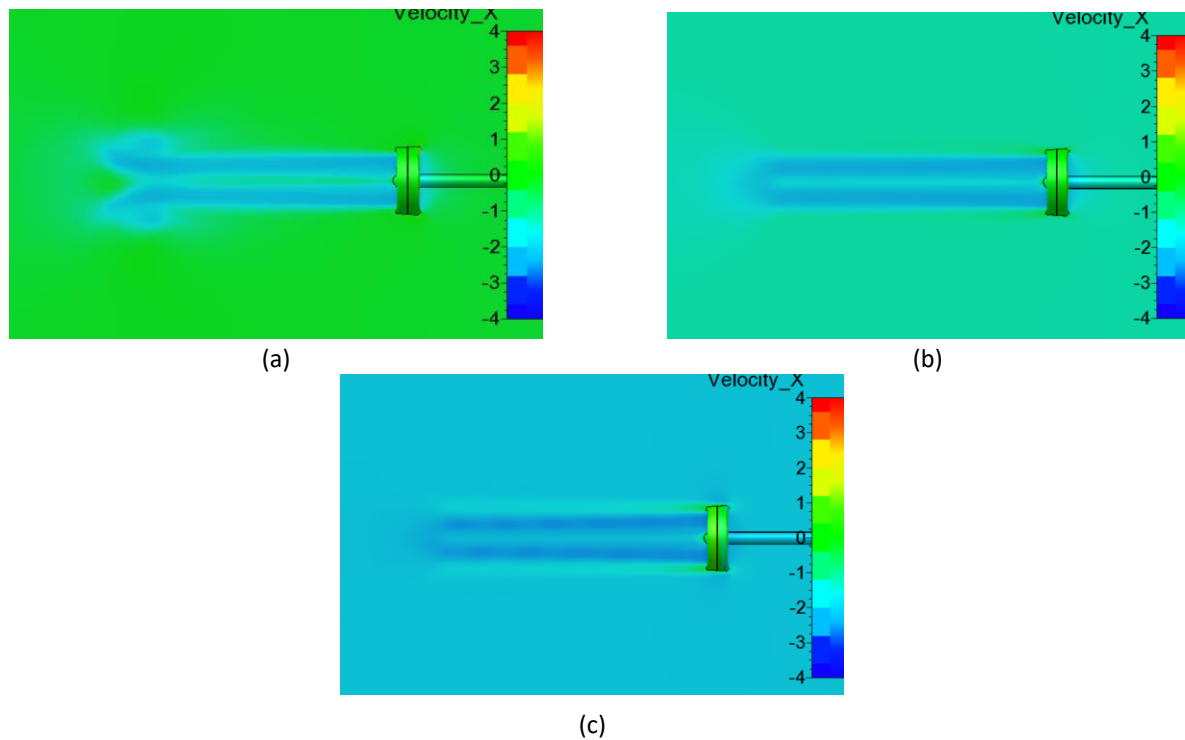
(a)

(b)

(c)

Fig. 9. Visualization of velocity on the propeller B4-70 with nozzle 19A (a) Velocity at J= 0.1 (b) Velocity at J= 0.5 (c) Velocity at J= 0.8

The visualization of the velocity of the B4-70 propeller with the nozzle 19A reinforces the results obtained from the CFD simulation in terms of pressure values. In the boss cap, there is significant pressure when J = 0.1, exceeding 1000 Pa, and similarly, when J = 0.5, it remains above 1000 Pa, but the pressure values are lower when J = 0.9, ranging from 250 Pa to 500 Pa. In this study, the B4-70 propeller with the 19A nozzle experiences high pressure at low speeds (J = 0.1) up to moderate speeds (J = 0.5), thus necessitating a solution to reduce this pressure. The visualization of the velocity of the B4-70 propeller with the 19A nozzle strengthens the CFD simulation results regarding pressure values. Starting from J = 0.1, the blade section exhibits axial induced velocities ranging from 2 m/s to 3 m/s, while at the boss cap of the propeller, the flow velocity remains between 0 m/s and 1 m/s. Meanwhile, in the blade section at J = 0.5, the axial induced velocity ranges from 2 m/s to 3 m/s, and in the boss cap of the propeller, there is flow with velocities ranging from 0 m/s to 2 m/s. At J = 0.8, the axial induced velocity in the blade section is 3 m/s to 4 m/s, although there is an increase in flow velocity at the boss cap of the propeller, ranging from 0 m/s to 3 m/s. In conclusion, for the B4-70 propeller without PBCF, it can be observed that as the value of J (advanced coefficient) increases, the flow velocity at the boss cap increases, while the flow velocity at the propeller blade remains constant.

3.2 Propeller Ka4-70 with Nozzle 19A

The results of propeller Ka4-70 with nozzle calculation are shown in Figure 10.

The open water test chart resulting from CFD simulations for the Ka4-70 propeller coupled with the nozzle 19A arrangement reveals that at J = 0.1, the K_T value stands at 0.549, which subsequently drops to 0.400 at J = 0.5, and hits its nadir at 0.015 when J = 1.0, as evidenced in Figure 10. Similarly, the $10K_Q$ value experiences a descent from 1.021 at J = 0.1 to 0.760 at J = 0.5, reaching its lowest point of 0.140 at J = 1.0. However, the efficiency (η_0) takes an inverse trajectory; starting from its lowest point at J = 0.1, it increases to 0.419 at J = 0.5, and culminates at 0.521 at J = 0.8. In summation,

the Ka4-70 propeller fitted with the 19A nozzle configuration demonstrates reduced efficiency during low speeds while showcasing elevated K_T and $10K_Q$ values. Moreover, it attains its peak η_0 value of 0.521 at J = 0.8 [29].
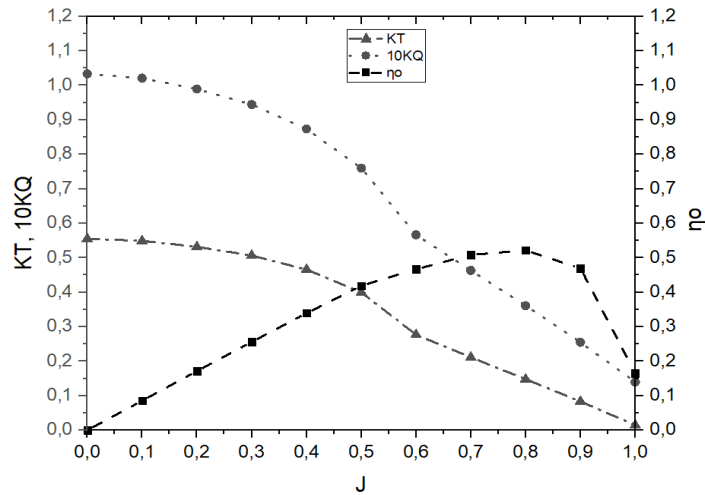

Fig. 10. Open water test diagram of Ka4-70 with nozzle 19A

The pressure visualization of the Ka4-70 propeller with nozzle 19A reinforces the outcomes of the CFD simulation in Figure 11. The results presented in the graphs indicate that at low speeds, J = 0, there is a high K_T value of 0.549; at moderate speeds, J = 0.5, the K_T value is 0.400; while at high speeds, J = 0.8, the K_T value is 0.148. In the region of the boss cap fins, significant pressure occurs at J = 0.1, exceeding 1000 Pa; similarly, at J = 0.5, the pressure is also above 1000 Pa, but the pressure value is lower at J = 0.8, being greater than or equal to 1000 Pa. This study highlights that the Ka4-70 Propeller with nozzle 19A experiences substantial pressure at low speeds, J = 0.1, up to high speeds, J = 0.8, indicating a need for a solution to reduce the pressure.

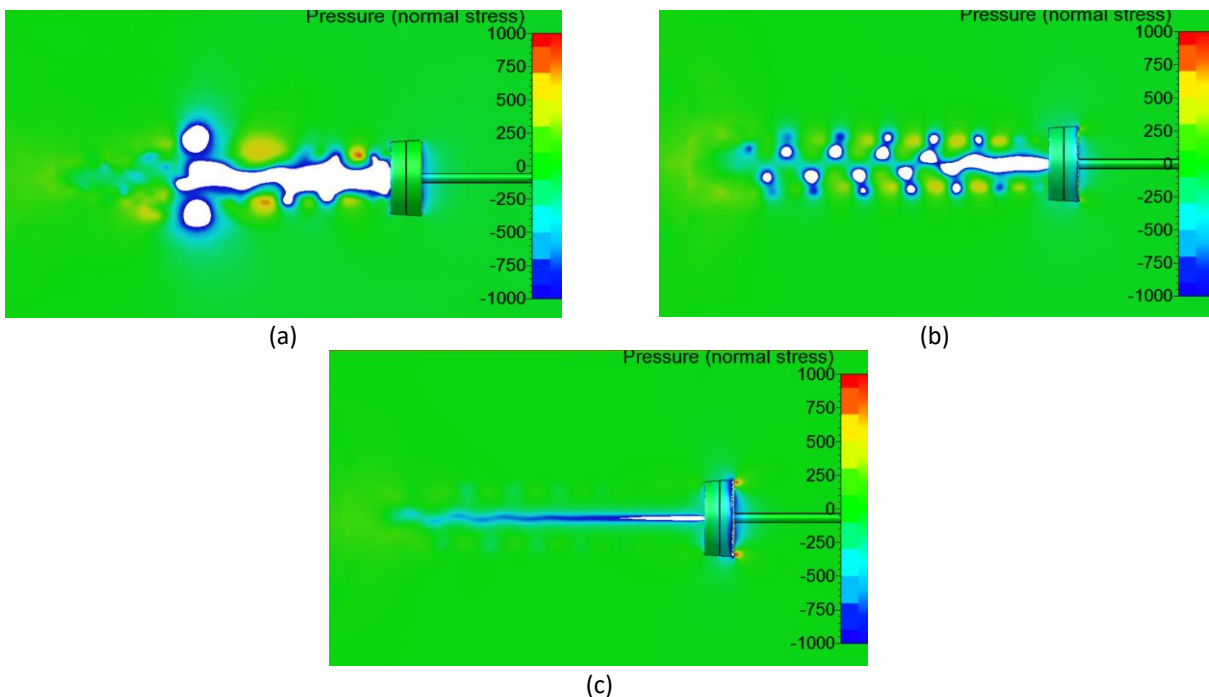(a)

(b)

(c)

Fig. 11. Visualization of pressure on the Ka4-70 propeller with nozzle 19A (a) Pressure at J= 0.1 (b) Pressure at J= 0.5 (c) Pressure at J= 0.8
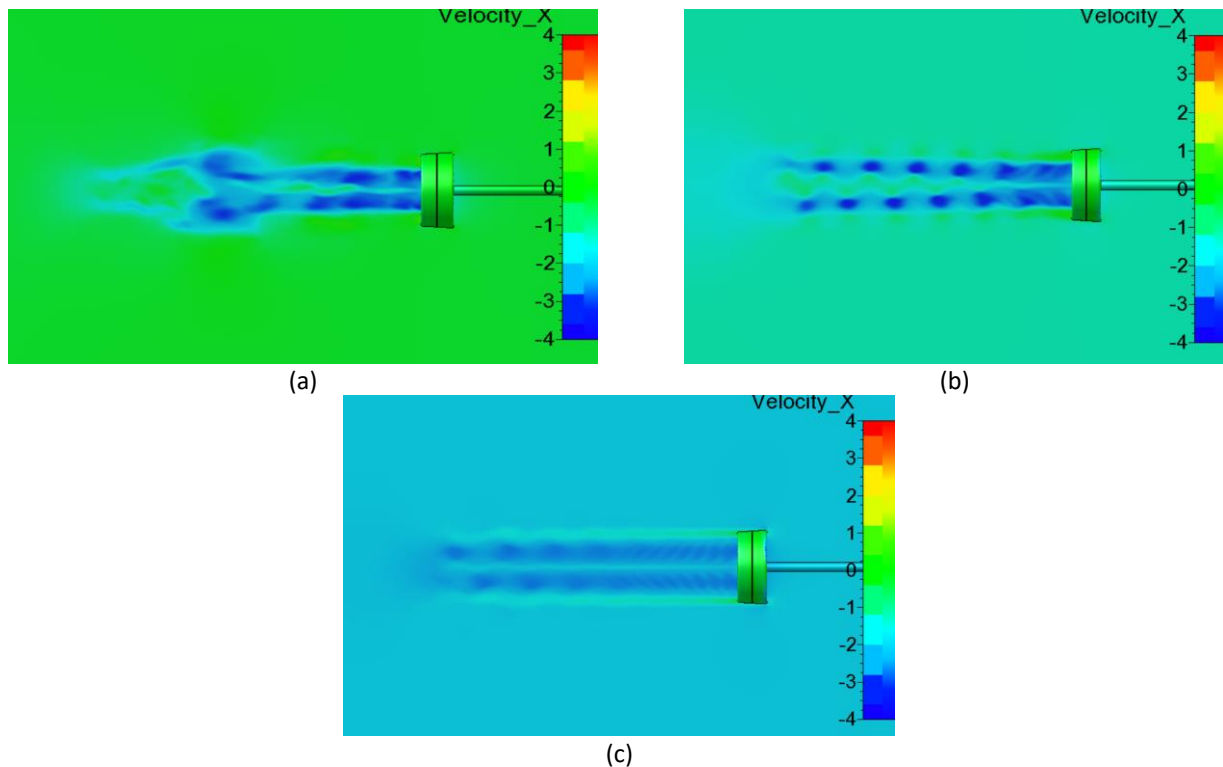
Fig. 12. Visualization of velocity on the propeller Ka4-70 with nozzle 19A (a) Velocity at J= 0.1 (b) Velocity at J= 0.5 (c) Velocity at J= 0.8

The visualization of the velocity of the Ka4-70 propeller with the nozzle 19A reinforces the results obtained from the CFD simulation in terms of pressure values. In the boss cap fin, there is significant pressure when J = 0.1, exceeding 1000 Pa, and similarly, when J = 0.5, it remains above 1000 Pa, but the pressure values are lower when J = 0.8, remaining above 1000 Pa. In this study, the Ka4-70 propeller without PBCF experiences high pressure at low speeds (J = 0.1) up to moderate speeds (J = 0.5), thus necessitating a solution to reduce this pressure. The visualization of the velocity of the Ka4-70 propeller with the nozzle 19A strengthens the CFD simulation results regarding pressure values. Starting from J = 0.1, the blade section exhibits axial induced velocities ranging from 3 m/s to 4 m/s, while at the boss cap of the propeller, the flow velocity remains between 0 m/s and 2 m/s. Meanwhile, in the blade section at J = 0.5, the axial induced velocity ranges from 3 m/s to 4 m/s, and in the boss cap of the propeller, there is flow with velocities ranging from 0 m/s to 2 m/s. At J = 0.9, the axial induced velocity in the blade section is 2 m/s to 3 m/s, although there is an increase in flow velocity at the boss cap of the propeller, ranging from 0 m/s to 1 m/s. In conclusion, for the Ka4-70 propeller with the nozzle 19A, it can be observed that as the value of J (advanced coefficient) increases, the flow velocity at the boss cap decreases, while the flow velocity at the propeller blade remains constant [22].

4. Propeller B4-70 and Ka4-70 with Nozzle and PBCF
4.1 Propeller B4-70 with Nozzle and PBCF

The results of Propeller B4-70 with nozzle 19A and BCF default calculation are shown in Figure 13.
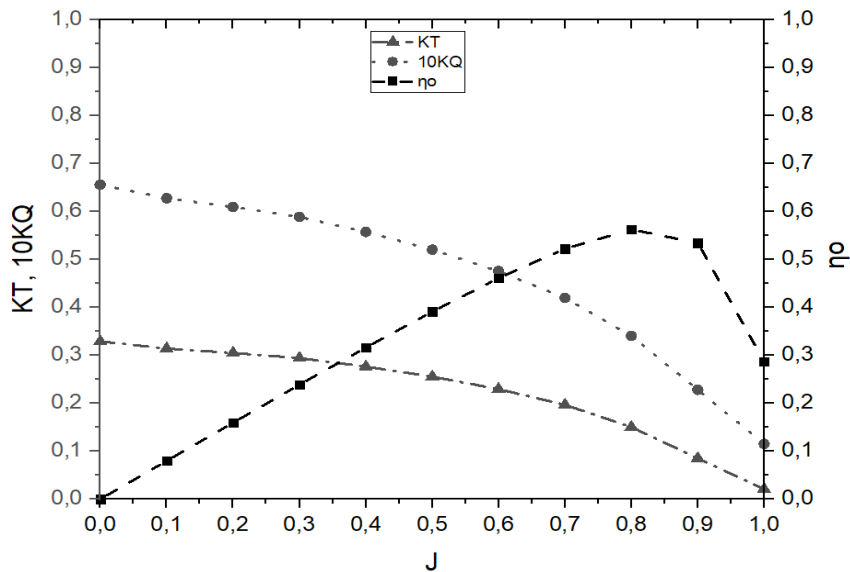
Fig. 13. Open water test diagram of B4-70 with nozzle 19A and BCF default

In Figure 13, At J = 0.1, the K_T value is 0.329 and decreases to 0.255 at J = 0.5, reaching its lowest value of 0.021 at J = 1.0. A similar trend is observed for $10K_Q$, with a value of 0.627 at J = 0.1 decreasing to 0.520 at J = 0.5 and reaching its lowest value of 0.115 at J = 1.0. However, the efficiency exhibits the opposite behaviour, as the lowest efficiency at J = 0.1 increases to 0.391 at J = 0.5 and reaches its peak value of 0.562 at J = 0.8. In conclusion, for the B4-70 propeller with the 19A nozzle and default boss cap fins, the efficiency is low at low speeds, while K_T and $10K_Q$ are high. The highest η_0 value achieved is 0.562 at J = 0.8 [30].

The pressure visualization of the B4-70 Propeller with nozzle 19A and BCF default reinforces the results of the CFD simulation in Figure 14. The outcomes presented in the graphs demonstrate that at low speeds, J = 0, there is a high K_T value of 0.329; at moderate speeds, J = 0.5, the K_T value is 0.255; while at high speeds, J = 0.8, the K_T value is 0.150. In the region of the boss cap fins, significant pressure occurs at J = 0.1, exceeding 1000 Pa; similarly, at J = 0.5, the pressure is 1000 Pa, but the pressure value is lower at J = 0.8, ranging from 250 to 500 Pa. This study highlights that the B4-70 Propeller with nozzle 19A and default Boss Cap Fins experiences substantial pressure at low speeds, J = 0.1, up to moderate speeds, J = 0.5, indicating a need for a solution to reduce the pressure.

The visualization of the velocity of the B4-70 propeller with the nozzle 19A and the BCF (Boss Cap Fins) default strengthens the results obtained from the CFD simulation in terms of pressure values. In the boss cap fin, there is significant pressure when J = 0.1, exceeding 1000 Pa, and similarly, when J = 0.5, it reaches 1000 Pa, but the pressure values are lower when J = 0.8, ranging from 250 Pa to 500 Pa. In this study, the B4-70 propeller with the 19A nozzle and the default BCF experiences high pressure at low speeds (J = 0.1) up to moderate speeds (J = 0.5), thus necessitating a solution to reduce this pressure. The visualization of the velocity of the B4-70 propeller with the 19A nozzle and the default BCF strengthens the CFD simulation results regarding pressure values. Starting from J = 0.1, the blade section exhibits axial induced velocities ranging from 2 m/s to 3 m/s, while at the boss cap of the propeller, the flow velocity remains between 0 m/s and 1 m/s. Meanwhile, in the blade section at J = 0.5, the axial induced velocity ranges from 2 m/s to 3 m/s, and in the boss cap of the propeller, there is flow with velocities ranging from 0 m/s to 2 m/s. At J = 0.8, the axial induced velocity in the blade section is 2 m/s to 3 m/s, although there is an increase in flow velocity at the boss cap of the propeller, ranging from 0 m/s to 2 m/s. In conclusion, for the B4-70 propeller with the nozzle 19A and the default BCF, it can be observed that as the value of J (advanced coefficient) increases, the flow velocity at the boss cap increases, while the flow velocity at the propeller blade

remains constant. Therefore, a solution is needed to address the increase in flow velocity at the boss cap.
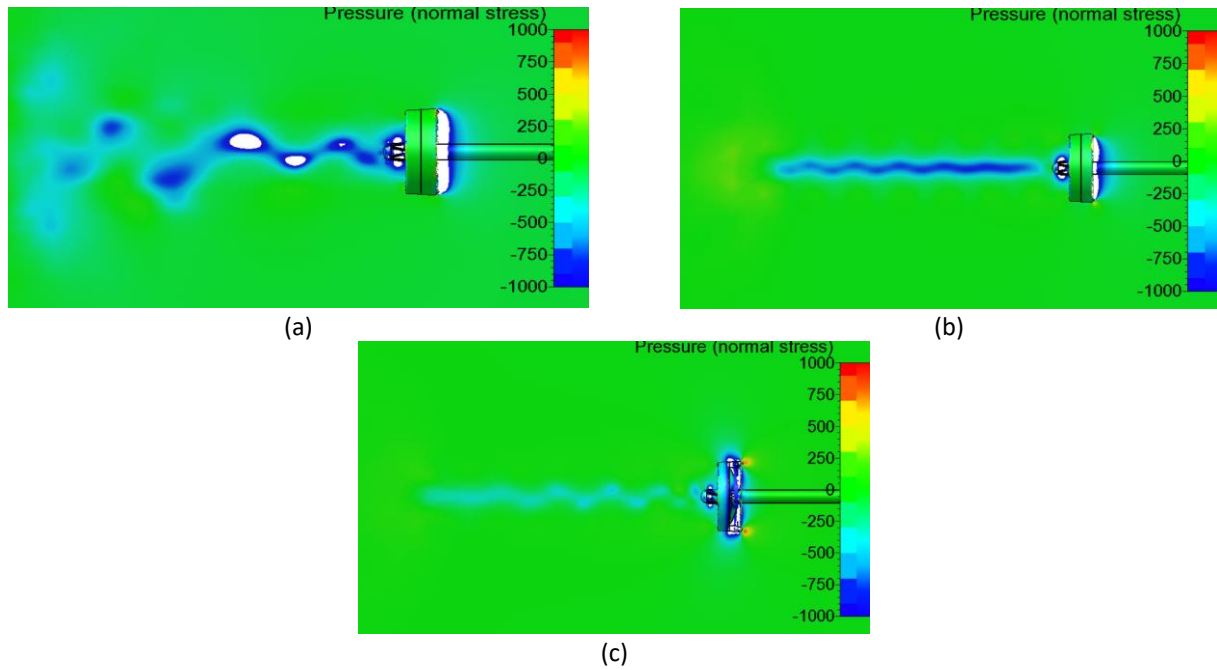

(a)

(b)

(c)

Fig. 14. Visualization of pressure on the B4-70 propeller with nozzle 19A and BCF default (a) Pressure at J= 0.1 (b) Pressure at J= 0.5 (c) Pressure at J= 0.8
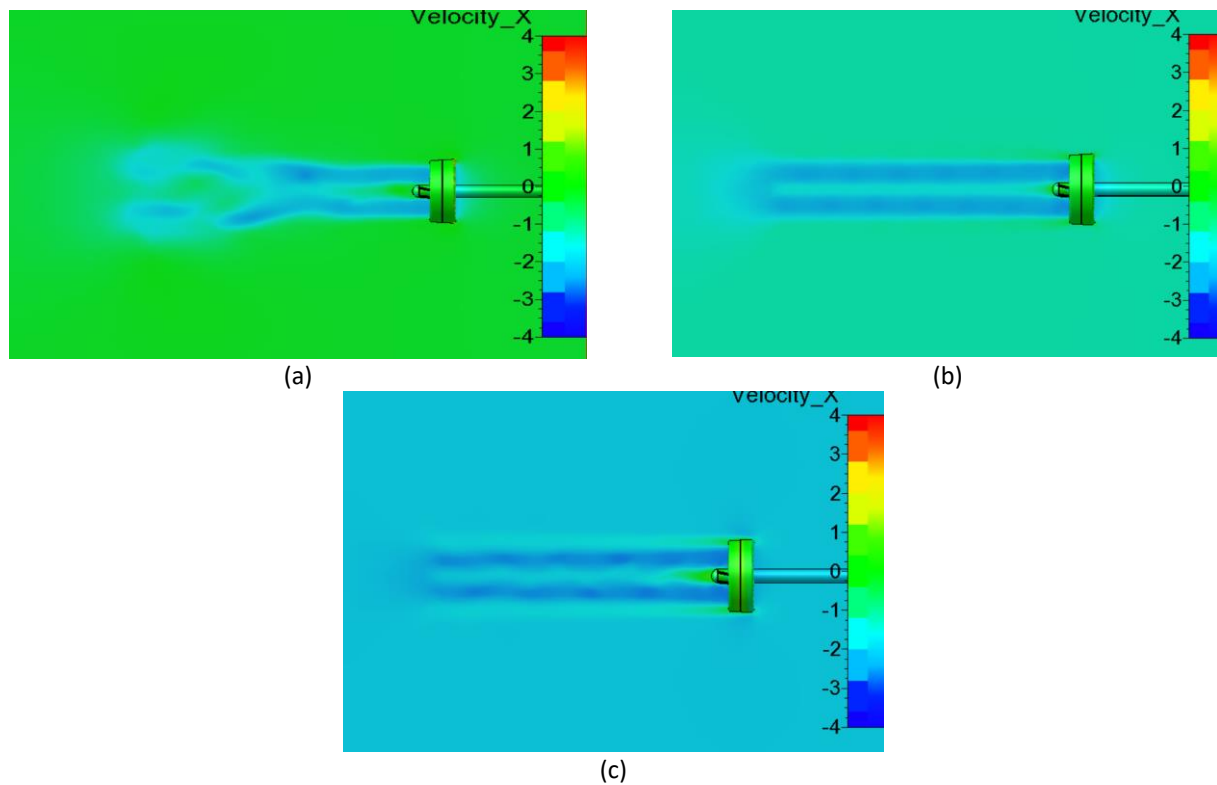

(a)

(b)

(c)

Fig. 15. Visualization of velocity on the B4-70 with nozzle 19A and BCF default (a) Velocity at J= 0.1 (b) Velocity at J= 0.5 (c) Velocity at J= 0.8

The results of Propeller B4-70 with nozzle 19A and BCF straight calculation are shown in Figure 16.
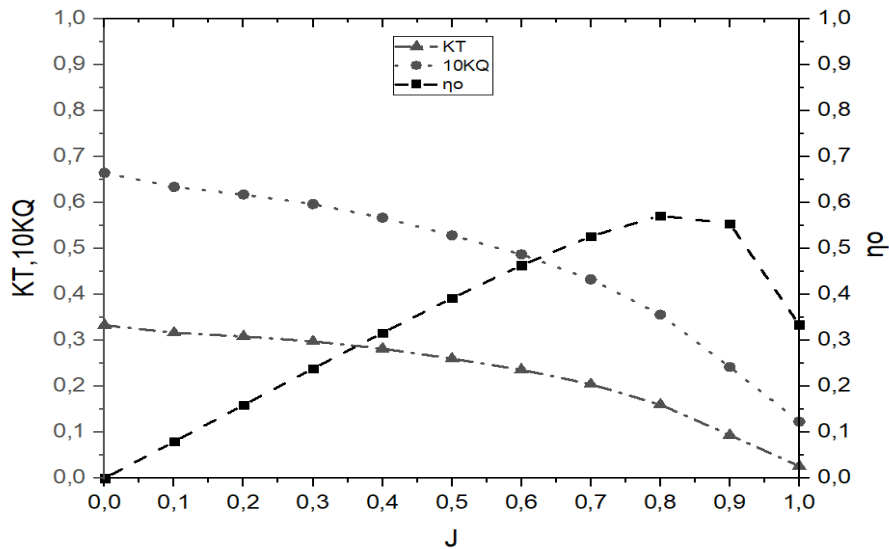

Fig. 16. Open water test diagram of B4-70 with nozzle 19A and BCF straight

The open water test graph for the B4-70 propeller with the nozzle 19A and straight BCF configuration is obtained from CFD simulations with the result illustrated in Figure 16. At J = 0.1, the K_T value is 0.316 and decreases to 0.260 at J = 0.5, reaching its lowest value of 0.026 at J = 1.0. Similarly, the $10K_Q$ value starts at 0.634 at J = 0.1 and decreases to 0.528 at J = 0.5, reaching its lowest value of 0.123 at J = 1.0. However, the efficiency exhibits the opposite behaviour, as the lowest efficiency at J = 0.1 increases to 0.391 at J = 0.5 and reaches its peak value of 0.571 at J = 0.8. In conclusion, for the B4-70 propeller with the nozzle 19A and straight BCF, the efficiency is low at low speeds, while K_T and $10K_Q$ are high. The highest η_0 value achieved is 0.571 at J = 0.8 [31].

The pressure visualization of the B4-70 Propeller with nozzle 19A and BCF straight reinforces the results of the CFD simulation Figure 17. The outcomes presented in the graphs demonstrate that at low speeds, J = 0, there is a high K_T value of 0.316; at moderate speeds, J = 0.5, the K_T value is 0.260; while at high speeds, J = 0.8, the K_T value is 0.159. In the region of the straight boss cap fins, significant pressure occurs at J = 0.1, exceeding 1000 Pa; similarly, at J = 0.5, the pressure is also above 1000 Pa, but the pressure value is lower at J = 0.8, ranging from 250 Pa to 500 Pa. This study highlights that the B4-70 Propeller with nozzle 19A and straight Boss Cap Fins experiences substantial pressure at low speeds, J = 0.1, up to moderate speeds, J = 0.5.

The visualization of the velocity of the B4-70 propeller with the nozzle 19A and the BCF straight strengthens the results obtained from the CFD simulation in terms of pressure values. In the boss cap fin, there is significant pressure when J = 0.1, exceeding 1000 Pa, and similarly, when J = 0.5, it remains above 1000 Pa, but the pressure values are lower when J = 0.8, ranging from 250 Pa to 500 Pa. In this study, the B4-70 propeller with the 19A nozzle and the straight BCF experiences high pressure at low speeds (J = 0.1) up to moderate speeds (J = 0.5), thus necessitating a solution to reduce this pressure. The visualization of the velocity of the B4-70 propeller with the 19A nozzle and the straight BCF strengthens the CFD simulation results regarding pressure values. Starting from J = 0.1, the blade section exhibits axial induced velocities ranging from 2 m/s to 3 m/s, while at the boss cap of the propeller, the flow velocity remains between 0 m/s and 1 m/s. Meanwhile, in the blade section at J = 0.5, the axial induced velocity ranges from 2 m/s to 3 m/s, and in the boss cap of the propeller, there is flow with velocities ranging from 0 m/s to 2 m/s. At J = 0.8, the axial induced velocity in the

blade section is 3 m/s to 4 m/s, although there is an increase in flow velocity at the boss cap of the propeller, ranging from 0 m/s to 2 m/s. In conclusion, for the B4-70 propeller with the 19A nozzle and the straight BCF, it can be observed that as the value of J (advanced coefficient) increases, the flow velocity at both the boss cap and the propeller blade increases.
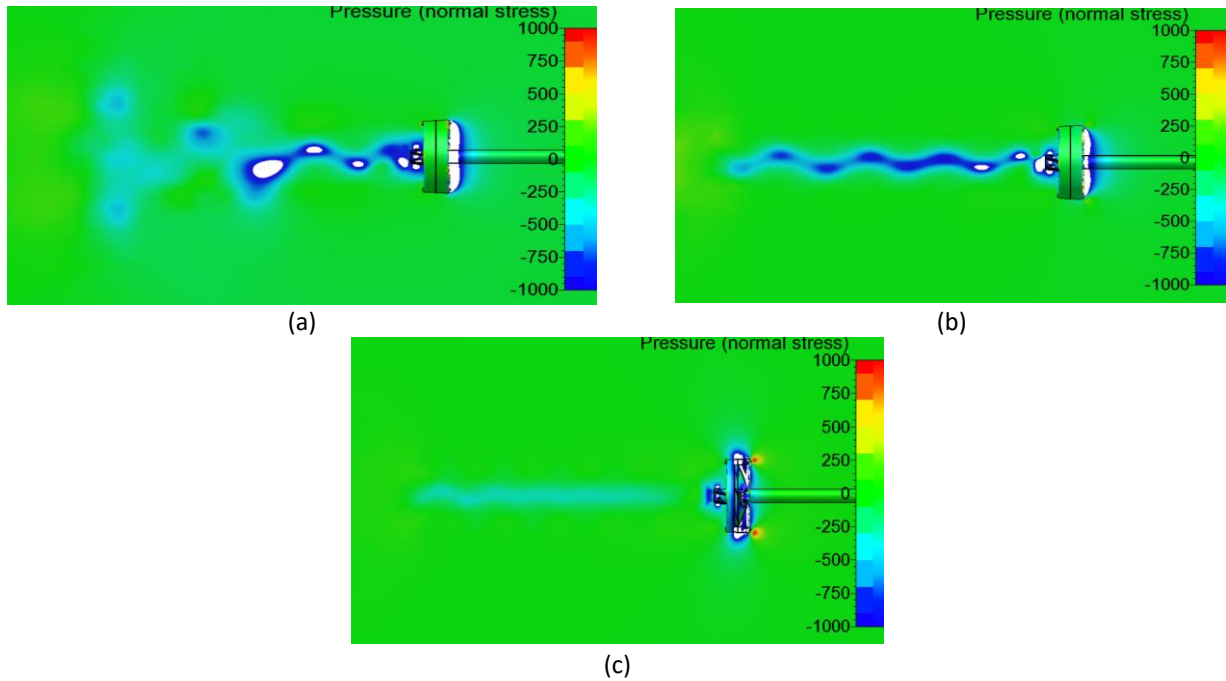

Fig. 17. Visualization of pressure on the B4-70 propeller with nozzle 19A and BCF straight (a) Pressure at J= 0.1 (b) Pressure at J= 0.5 (c) Pressure at J= 0.8
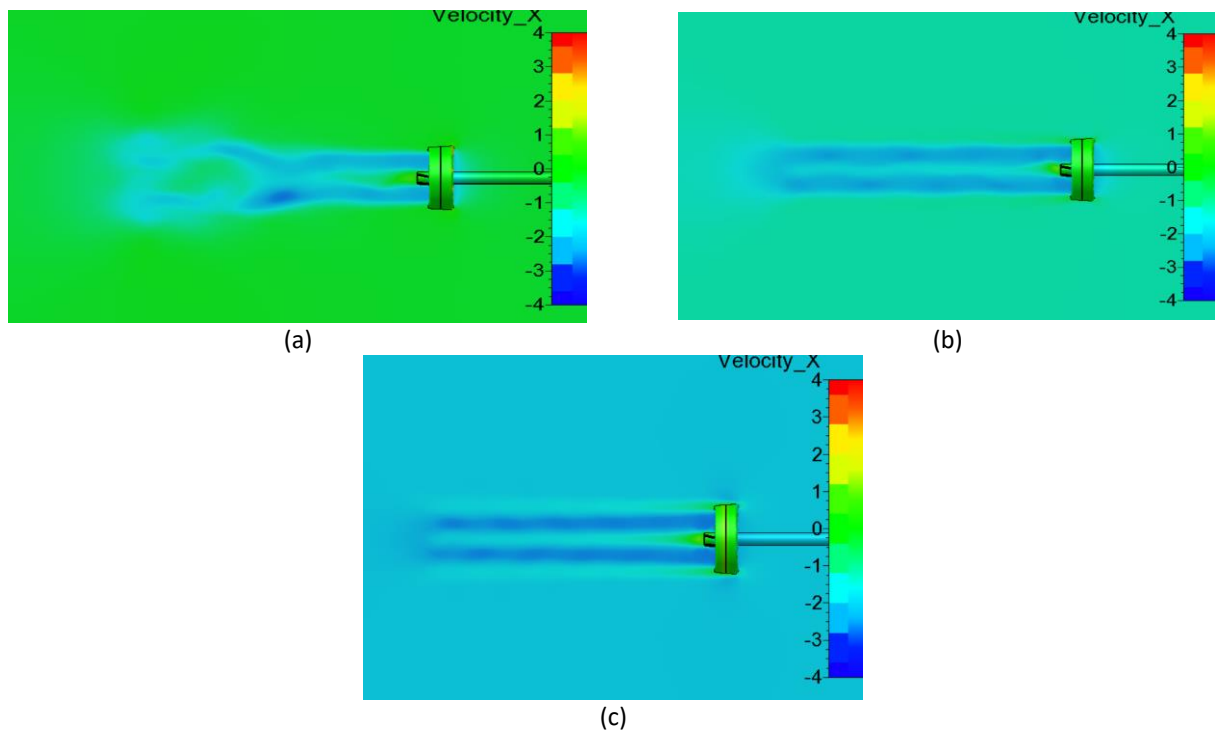

Fig. 18. Visualization of velocity on the propeller B4-70 with nozzle 19A and BCF straight (a) Velocity at J= 0.1 (b) Velocity at J= 0.5 (c) Velocity at J= 0.8

The results of Propeller B4-70 with nozzle 19A and BCF convergent calculation are shown in Figure 19.
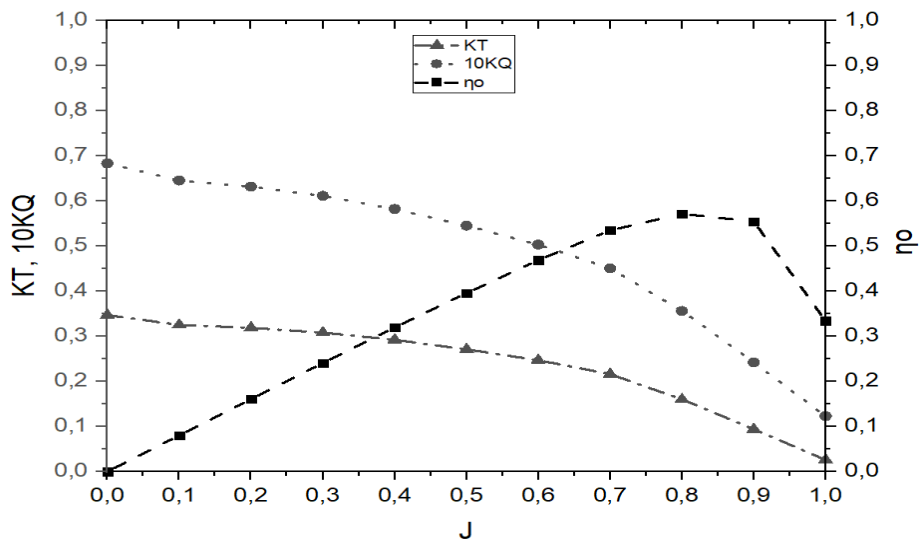

Fig. 19. Open water test diagram of B4-70 with nozzle 19A and BCF convergent

The open water test graph for the B4-70 propeller with the nozzle 19A and BCF convergent configuration is obtained from CFD simulations, as conclude in Figure 19, shows that at J = 0.1, the K_T value is 0.325 and decreases to 0.271 at J = 0.5, reaching its lowest value of 0.044 at J = 1.0. Similarly, the $10K_Q$ value starts at 0.645 at J = 0.1 and decreases to 0.545 at J = 0.5, reaching its lowest value of 0.184 at J = 1.0. However, the efficiency exhibits the opposite behaviour, as the lowest efficiency at J = 0.1 increases to 0.396 at J = 0.5 and reaches its peak value of 0.592 at J = 0.9. In conclusion, for the B4-70 propeller with the 19A nozzle and convergent BCF, the efficiency is low at low speeds, while K_T and $10K_Q$ are high. The highest η_0 value achieved is 0.592 at J = 0.9 [32].

The pressure visualization of the B4-70 Propeller with nozzle 19A and convergent Boss Cap Fins reinforces the results of the CFD simulation in Figure 20. The outcomes presented in the graphs demonstrate that at low speeds, J = 0, there is a high K_T value of 0.325; at moderate speeds, J = 0.5, the K_T value is 0.271; while at high speeds, J = 0.9, the K_T value is 0.113. In the region of the convergent boss cap fins, significant pressure occurs at J = 0.1, exceeding 1000 Pa; similarly, at J = 0.5, the pressure is also above 1000 Pa, but the pressure value is lower at J = 0.9, ranging from 250 Pa to 500 Pa. This study highlights that the B4-70 Propeller with nozzle 19A and convergent Boss Cap Fins experiences substantial pressure at low speeds, J = 0.1, up to moderate speeds, J = 0.5, indicating a need for a solution to reduce the pressure.

The visualization of the velocity of the B4-70 propeller with the 19A nozzle and the convergent BCF (Boss Cap Fins) strengthens the results obtained from the CFD simulation in terms of pressure values. In the boss cap fin, there is significant pressure when J = 0.1, exceeding 1000 Pa, and similarly, when J = 0.5, it remains above 1000 Pa, but the pressure values are lower when J = 0.9, ranging from 250 Pa to 500 Pa. In this study, the B4-70 propeller without PBCF experiences high pressure at low speeds (J = 0.1) up to moderate speeds (J = 0.5). The visualization of the velocity of the B4-70 propeller with the 19A nozzle and the convergent BCF strengthens the CFD simulation results regarding pressure values. Starting from J = 0.1, the blade section exhibits axial induced velocities ranging from 2 m/s to 3 m/s, while at the boss cap of the propeller, the flow velocity remains between 0 m/s and 1 m/s. Meanwhile, in the blade section at J = 0.5, the axial induced velocity ranges from 2 m/s to 3 m/s, and in the boss cap of the propeller, there is flow with velocities ranging from 0 m/s to 1 m/s.

At J = 0.8, the axial induced velocity in the blade section is 3 m/s to 4 m/s, although there is an increase in flow velocity at the boss cap of the propeller, ranging from 0 m/s to 1 m/s. In conclusion, for the B4-70 propeller with the nozzle 19A and the convergent BCF, it can be observed that as the value of J (advanced coefficient) increases, the flow velocity at the boss cap increases, while the flow velocity at the propeller blade remains constant.
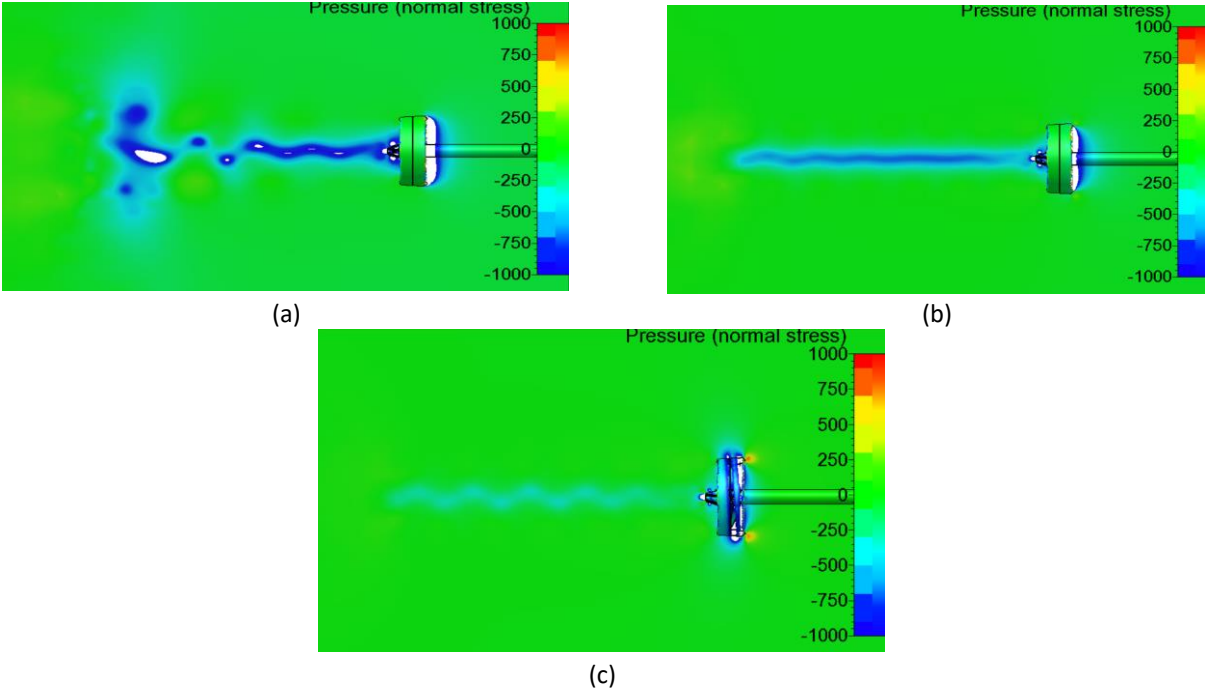

(a)

(b)

(c)

Fig. 20. Visualization of pressure on the B4-70 propeller with nozzle 19A and BCF convergent (a) Pressure at J= 0.1 (b) Pressure at J= 0.5 (c) Pressure at J= 0.9
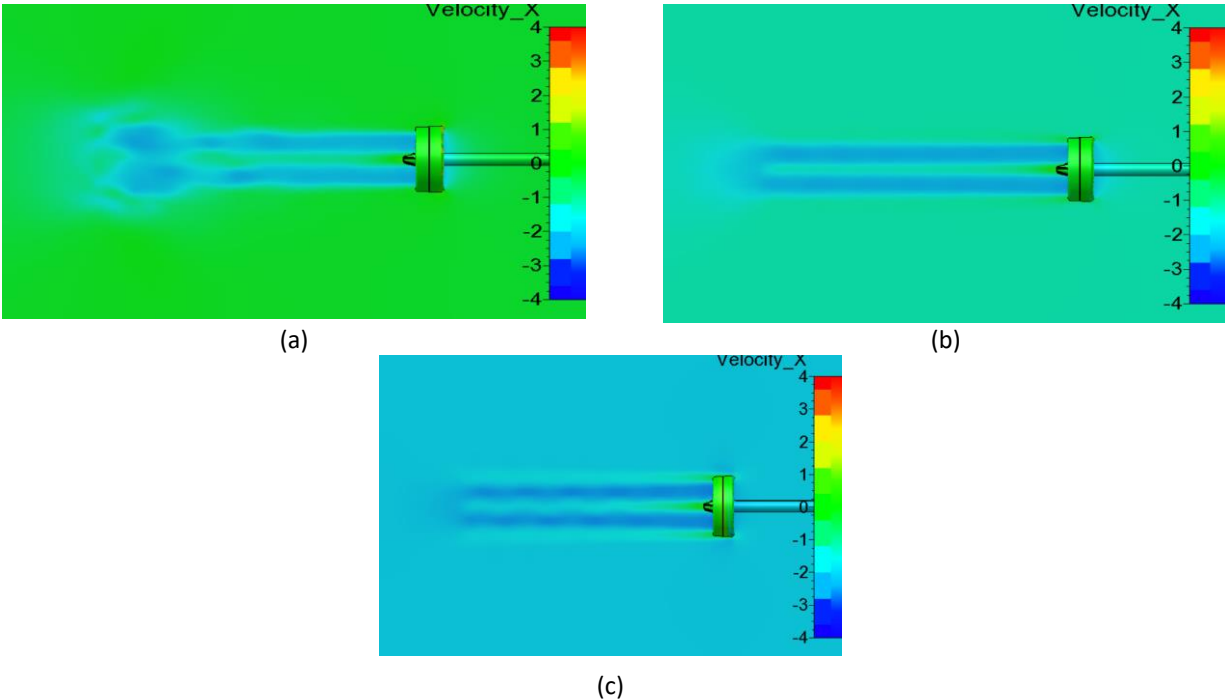

(a)

(b)

(c)

Fig. 21. Visualization of velocity on the propeller B4-70 with nozzle 19A and BCF convergent (a) Velocity at J= 0.1 (b) Velocity at J= 0.5 (c) Velocity at J= 0.8

The results of Propeller B4-70 with nozzle 19A and BCF divergent calculation are shown in Figure 22.
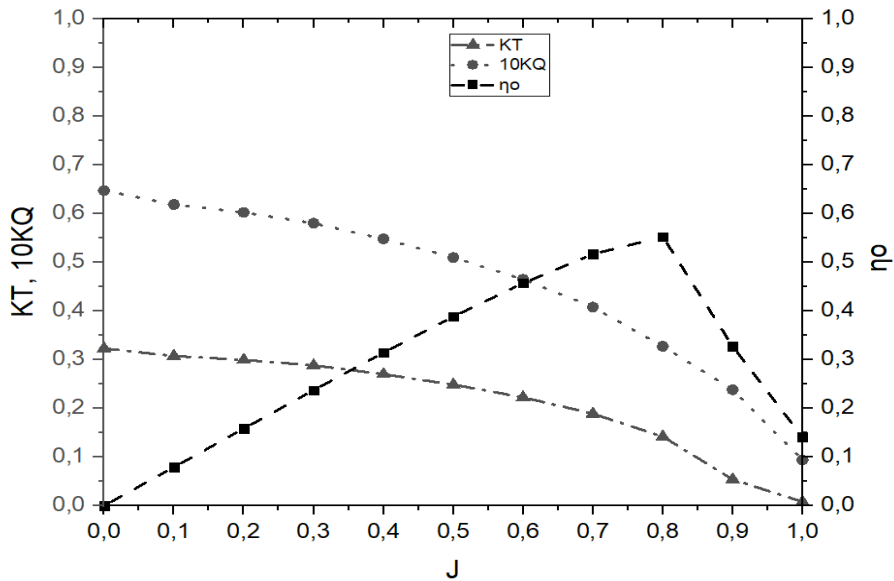

Fig. 22. Open water test diagram of B4-70 with nozzle 19A and BCF divergent

The open water test graph for the B4-70 propeller with the BCF default configuration is obtained from CFD simulations shown in Figure 22. At J = 0.1, the K_T value is 0.307 and decreases to 0.248 at J = 0.5, reaching its lowest value of 0.008 at J = 1.0. Similarly, the $10K_Q$ value starts at 0.618 at J = 0.1 and decreases to 0.509 at J = 0.5, reaching its lowest value of 0.094 at J = 1.0. However, the efficiency exhibits the opposite behaviour, as the lowest efficiency at J = 0.1 increases to 0.388 at J = 0.5 and reaches its peak value of 0.552 at J = 0.8. In conclusion, for the B4-70 propeller with the default BCF, the efficiency is low at low speeds, while K_T and $10K_Q$ are high. The highest η_0 value achieved is 0.552 at J = 0.8 [33].

The pressure visualization of the B4-70 Propeller with nozzle 19A and divergent Boss Cap Fins reinforces the results of the CFD simulation in Figure 23. The outcomes presented in the graphs demonstrate that at low speeds, J = 0, there is a high K_T value of 0.323; at moderate speeds, J = 0.5, the K_T value is 0.248; while at high speeds, J = 0.8, the K_T value is 0.142. In the region of the divergent boss cap fins, significant pressure occurs at J = 0.1, exceeding 1000 Pa; similarly, at J = 0.5, the pressure is also above 1000 Pa, but the pressure value is lower at J = 0.9, ranging from 250 to 500 Pa. This study highlights that the B4-70 Propeller with nozzle 19A and divergent Boss Cap Fins experiences substantial pressure at low speeds, J = 0.1, up to moderate speeds, J = 0.5.

The visualization of the velocity of the B4-70 propeller with the nozzle 19A and the BCF (Boss Cap Fins) divergent strengthens the results obtained from the CFD simulation in terms of pressure values. In the boss cap fin, there is significant pressure when J = 0.1, exceeding 1000 Pa, and similarly, when J = 0.5, it remains above 1000 Pa, but the pressure values are lower when J = 0.8, ranging from 250 Pa to 500 Pa. In this study, the B4-70 propeller with the 19A nozzle and the divergent BCF experiences high pressure at low speeds (J = 0.1) up to moderate speeds (J = 0.5), thus necessitating a solution to reduce this pressure. The visualization of the velocity of the B4-70 propeller without PBCF strengthens the CFD simulation results regarding pressure values. Starting from J = 0.1, the blade section exhibits induced axial velocities ranging from 2 m/s to 3 m/s, while at the boss cap of the propeller, the flow velocity remains between 0 m/s and 1 m/s. Meanwhile, in the blade section at J = 0.5, the induced axial velocity ranges from 2 m/s to 3 m/s, and in the boss cap of the propeller,

there is flow with velocities ranging from 0 m/s to 1 m/s. At J = 0.8, the induced axial velocity in the blade section is 3 m/s to 4 m/s, although there is an increase in flow velocity at the boss cap of the propeller, ranging from 0 m/s to 1 m/s. In conclusion, for the B4-70 propeller with the 19A nozzle and the divergent BCF, it can be observed that there is an increase in axial induced velocity at the propeller blade, but it does not result in an increase in velocity at the boss cap fins [34].
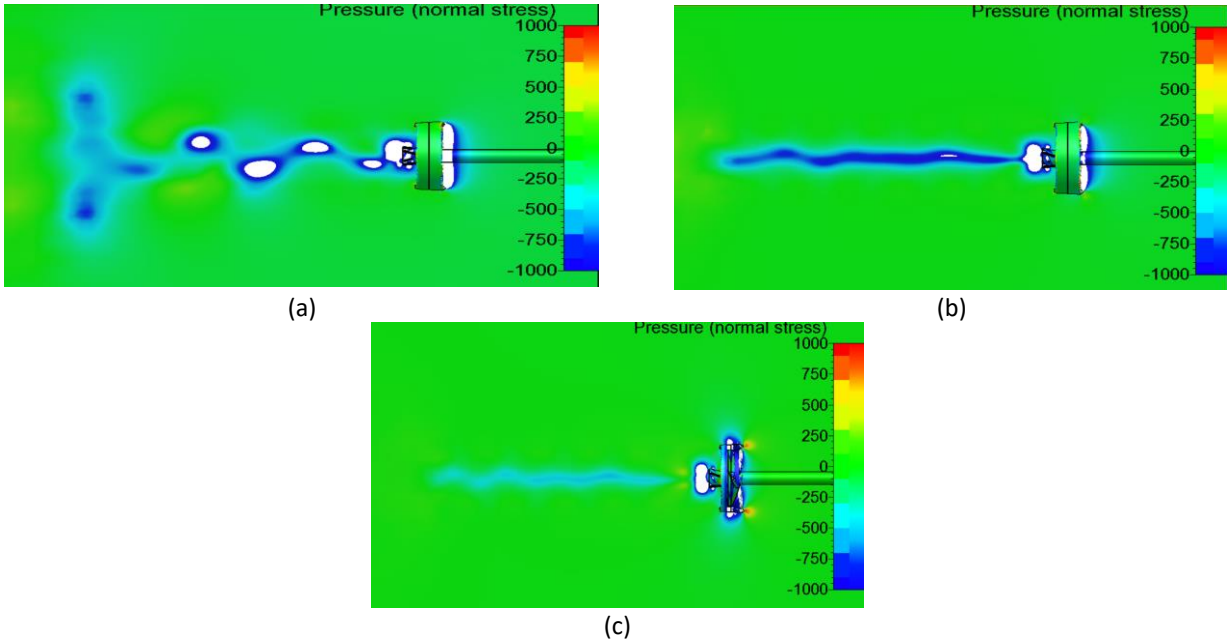

(a)

(b)

(c)

Fig. 23. Visualization of pressure on the B4-70 propeller with nozzle 19A and BCF divergent (a) Pressure at J= 0.1 (b) Pressure at J= 0.5 (c) Pressure at J= 0.8
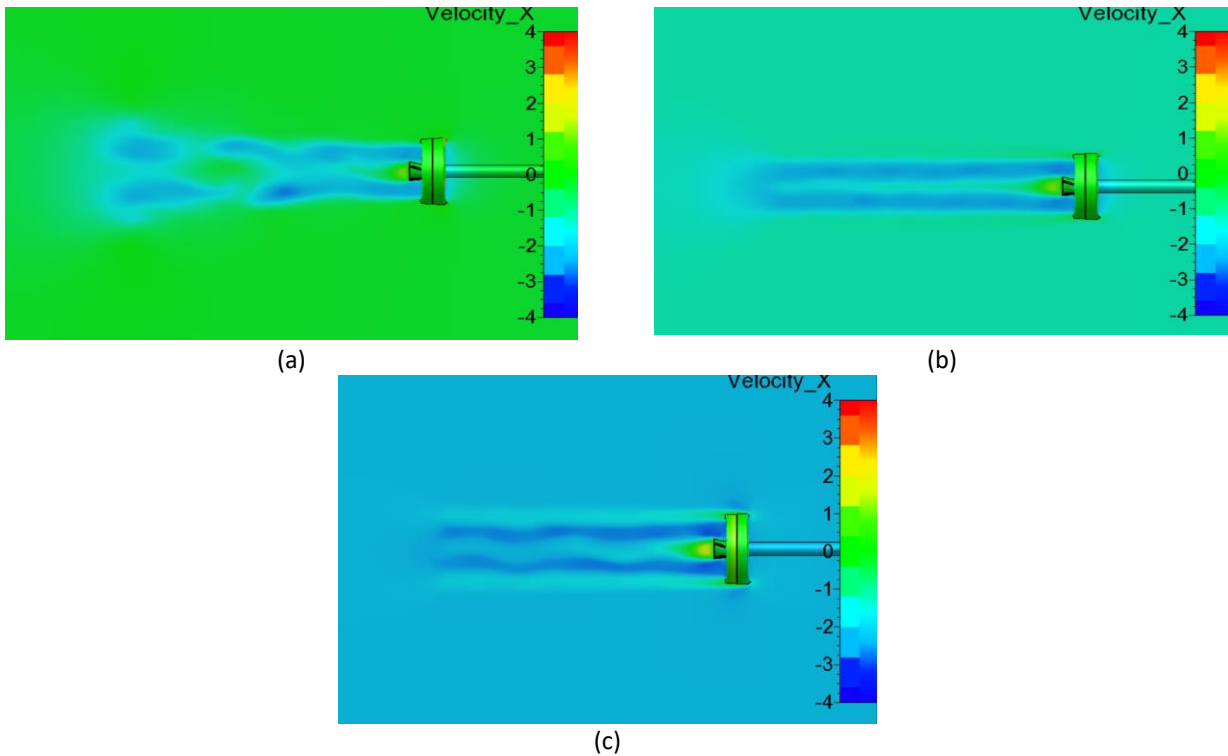

(a)

(b)

(c)

Fig. 24. Visualization of velocity on the velocity propeller B4-70 with nozzle 19A and BCF divergent (a) Velocity at J= 0.1 (b) Velocity at J= 0.5 (c) Velocity at J= 0.9

4.2 Propeller Ka4-70 with Nozzle and PBCF

The results of propeller Ka4-70 with nozzle 19A and BCF default calculation are shown in Figure 25.
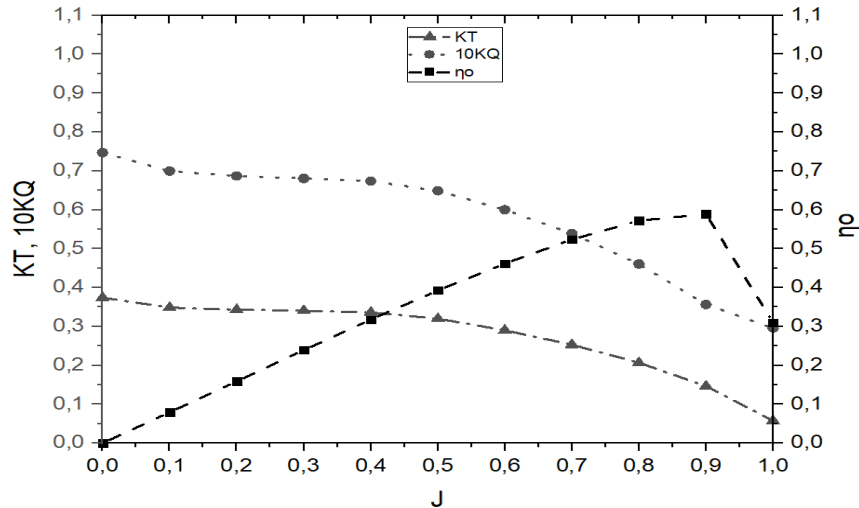

Fig. 25. Open water test diagram of Ka4-70 nozzle 19A and BCF default

The open water test graph for the Ka4-70 propeller with the default boss cap fins, obtained from CFD simulations illustrated in Figure 25 shows that at J = 0.1, the K_T value is 0.349 and decreases to 0.320 at J = 0.5, reaching its lowest point at J = 1.0 with a value of 0.058. Similarly, the $10K_Q$ value starts at 0.700 at J = 0.1, decreases to 0.649 at J = 0.5, and reaches its lowest point at J = 1.0 with a value of 0.296. However, the efficiency value behaves differently, as the lowest efficiency at J = 0.1 increases at J = 0.5, reaching a peak efficiency of 0.589 at J = 0.9. In conclusion, for the Ka4-70 propeller with the default boss cap fins, at low velocities, the efficiency is low while the K_T and $10K_Q$ values are high. The highest η_0 value is 0.589 at J = 0.9 [35].

The pressure visualization of the Ka4-70 Propeller with nozzle 19A and Boss Cap Fins default reinforces the results of the CFD simulation in Figure 26. The outcomes presented in the graphs demonstrate that at low speeds, J = 0, there is a high K_T value of 0.349; at moderate speeds, J = 0.5, the K_T value is 0.320; while at high speeds, J = 0.9, the K_T value is 0.147. In the region of the default boss cap fins, significant pressure occurs at J = 0.1, exceeding 1000 Pa; similarly, at J = 0.5, the pressure is also above 1000 Pa, but the pressure value is lower at J = 0.9, ranging from 250 to 500 Pa. This study highlights that the Ka4-70 Propeller with nozzle 19A and default Boss Cap Fins experiences substantial pressure at low speeds, J = 0.1, up to moderate speeds, J = 0.5, indicating a need for a solution to reduce the pressure.

The visualization of the velocity of the Ka4-70 propeller with the nozzle 19A and the BCF (Boss Cap Fins) default strengthens the results obtained from the CFD simulation in terms of pressure values. In the boss cap fin, there is significant pressure when J = 0.1, exceeding 1000 Pa, and similarly, when J = 0.5, it remains above 1000 Pa, but the pressure values are lower when J = 0.9, ranging from 250 Pa to 500 Pa. In this study, the Ka4-70 propeller without PBCF experiences high pressure at low speeds (J = 0.1) up to moderate speeds (J = 0.5), thus necessitating a solution to reduce this pressure. The visualization of the velocity of the Ka4-70 propeller with the 19A nozzle and the default BCF strengthens the CFD simulation results regarding pressure values. Starting from J = 0.1, the blade section exhibits induced axial velocities ranging from 2 m/s to 3 m/s, while at the boss cap of the propeller, the flow velocity remains between 0 m/s and 2 m/s. Meanwhile, in the blade section at J

= 0.5, the induced axial velocity ranges from 3 m/s to 4 m/s, and in the boss cap of the propeller, there is flow with velocities ranging from 0 m/s to 3 m/s. At J = 0.9, the induced axial velocity in the blade section is 3 m/s to 4 m/s, although there is an increase in flow velocity at the boss cap of the propeller, ranging from 0 m/s to 3 m/s. In conclusion, for the Ka4-70 propeller with the 19A nozzle and the default BCF, it can be observed that as the value of J (advanced coefficient) increases, the flow velocity at both the boss cap and the propeller blade increases.
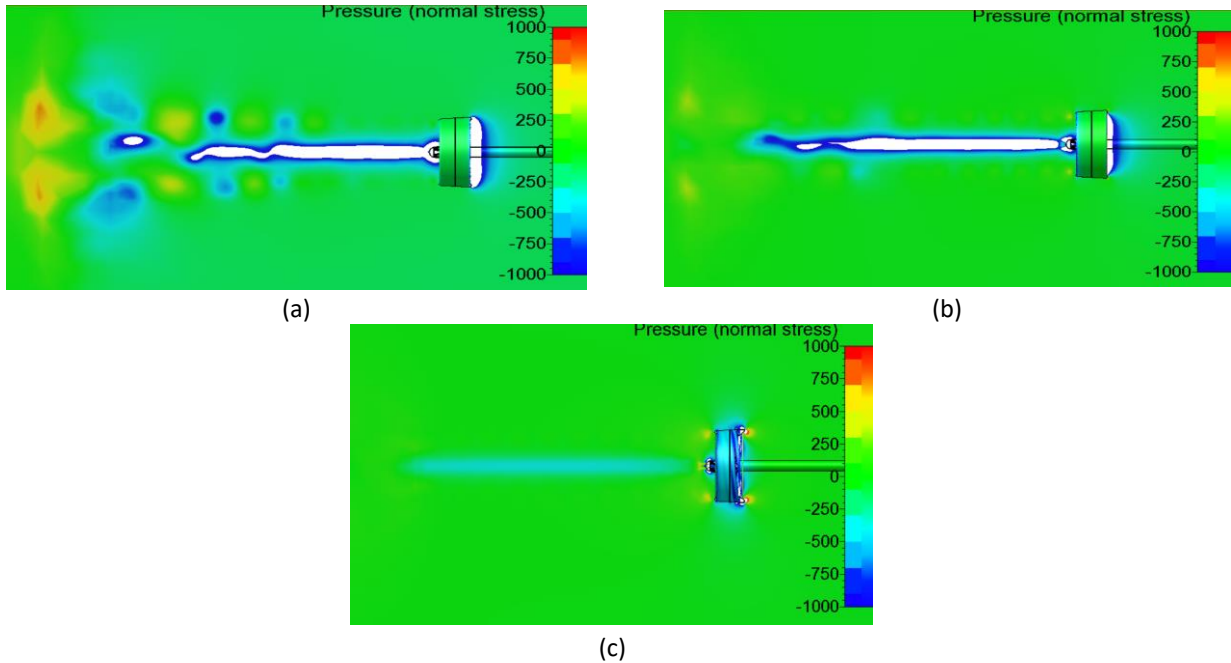

(a)

(b)

(c)

Fig. 26. Visualization of pressure on the Ka4-70 propeller with nozzle 19A and BCF default (a) Pressure at J= 0.1 (b) Pressure at J= 0.5 (c) Pressure at J= 0.9
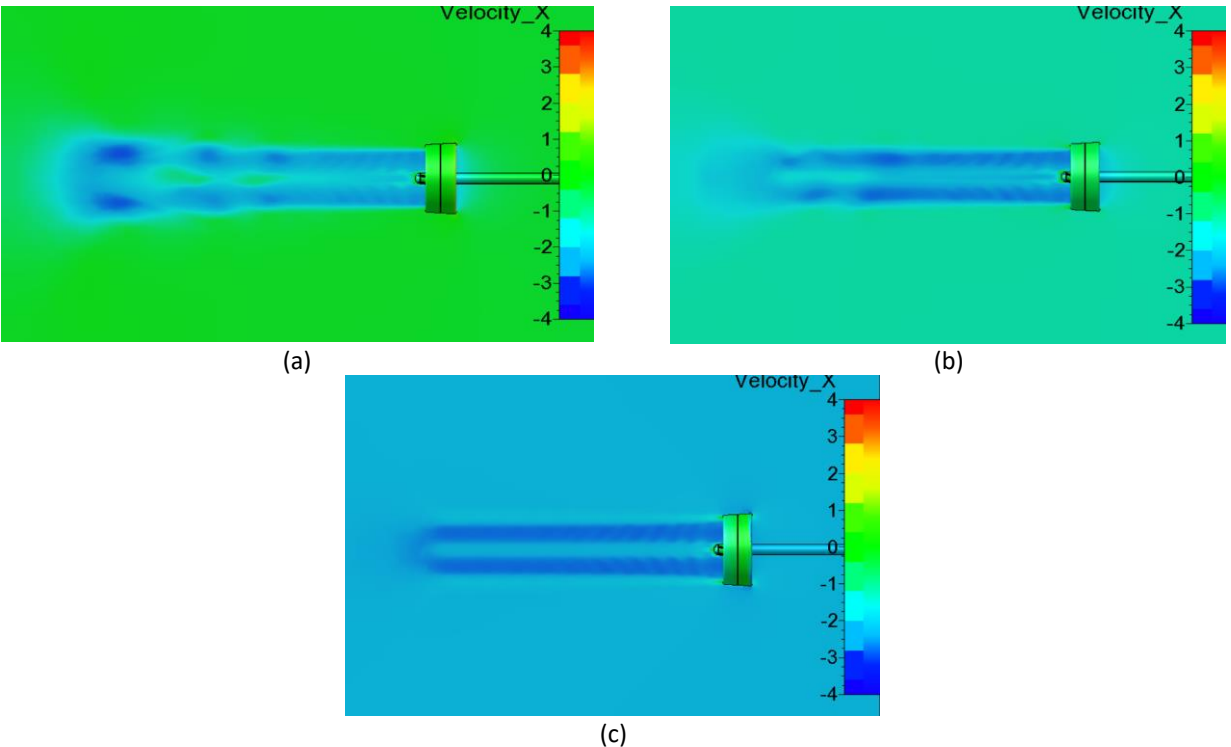

(a)

(b)

(c)

Fig. 27. Visualization of velocity on the propeller Ka4-70 with nozzle 19A and BCF default (a) Velocity at J= 0.1 (b) Velocity at J= 0.5 (c) Velocity at J= 0.9

The results of propeller Ka4-70 with nozzle 19A and BCF straight calculation are shown in Figure 28.
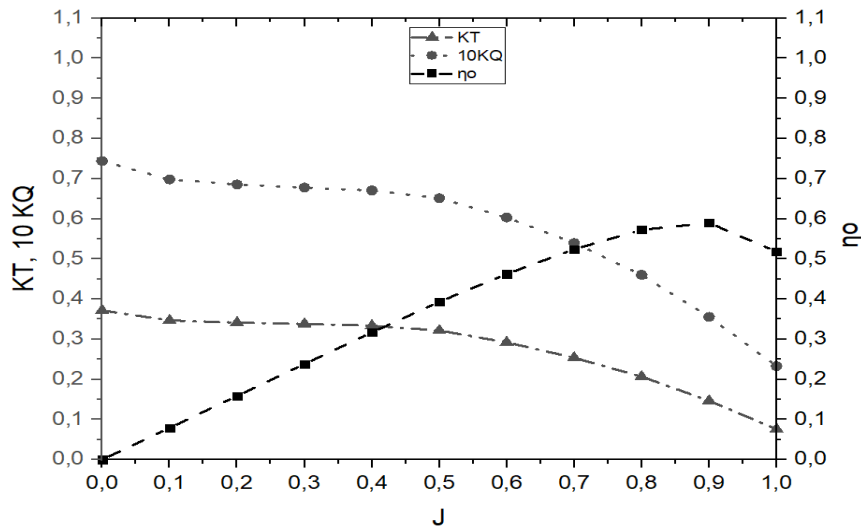

Fig. 28. Open water test diagram of Ka4-70 nozzle 19A and BCF straight

The open water test graph of the Ka4-70 Propeller with nozzle 19A and BCF straight, obtained from CFD simulations illustrated in Figure 28 shows that at J = 0.1, the value of K_T is 0.347 and decreases to 0.322 at J = 0.5, reaching its lowest point at J = 1.0 with a value of 0.076. A similar trend is observed for the value of $10K_Q$, where it is 0.698 at J = 0.1 and decreases to 0.651 at J = 0.5, reaching its lowest value at J = 1.0 with a value of 0.233. However, the efficiency behaves differently, as the lowest value at J = 0.1 increases at J = 0.5, reaching the peak efficiency of 0.590 at J = 0.9. Therefore, it can be concluded that for the Ka4-70 Propeller with nozzle 19A and BCF straight, at low speeds, the efficiency is also low but the values of K_T and $10K_Q$ are high. The highest value of η_0 is 0.590 at J = 0.9 [36].

The pressure visualization of the Ka4-70 Propeller with nozzle 19A and BCF straight reinforces the results of the CFD simulation in Figure 29. The outcomes presented in the graphs demonstrate that at low speeds, J = 0, there is a high K_T value of 0.347; at moderate speeds, J = 0.5, the K_T value is 0.322; while at high speeds, J = 0.9, the K_T value is 0.146. In the region of the straight boss cap fins, significant pressure occurs at J = 0.1, exceeding 1000 Pa; similarly, at J = 0.5, the pressure is also above 1000 Pa, but the pressure value is lower at J = 0.9, ranging from 250 to 500 Pa. This study highlights that the Ka4-70 Propeller with nozzle 19A and straight Boss Cap Fins experiences substantial pressure at low speeds, J = 0.1, up to moderate speeds, J = 0.5, indicating a need for a solution to reduce the pressure.

The visualization of the velocity of the Ka4-70 propeller with the nozzle 19A and the straight BCF (Boss Cap Fins) strengthens the results obtained from the CFD simulation in terms of pressure values. In the boss cap fin, there is significant pressure when J = 0.1, exceeding 1000 Pa, and similarly, when J = 0.5, it remains above 1000 Pa, but the pressure values are lower when J = 0.9, ranging from 250 Pa to 500 Pa. In this study, the Ka4-70 propeller with the 19A nozzle and the straight BCF experiences high pressure at low speeds (J = 0.1) up to moderate speeds (J = 0.5), thus necessitating a solution to reduce this pressure. The visualization of the velocity of the Ka4-70 propeller with the 19A nozzle and the straight BCF strengthens the CFD simulation results regarding pressure values. Starting from J = 0.1, the blade section exhibits induced axial velocities ranging from 2 m/s to 3 m/s, while at the boss cap of the propeller, the flow velocity remains between 0 m/s and 1 m/s. Meanwhile, in the blade section at J = 0.5, the induced axial velocity ranges from 3 m/s to 4 m/s, and in the boss cap of the

propeller, there is flow with velocities ranging from 0 m/s to 3 m/s. At J = 0.9, the induced axial velocity in the blade section is 3 m/s to 4 m/s, although there is an increase in flow velocity at the boss cap of the propeller, ranging from 0 m/s to 3 m/s. In conclusion, for the Ka4-70 propeller with the 19A nozzle and the straight BCF, it can be observed that as the value of J (advanced coefficient) increases, the flow velocity at both the boss cap and the propeller blade increases.
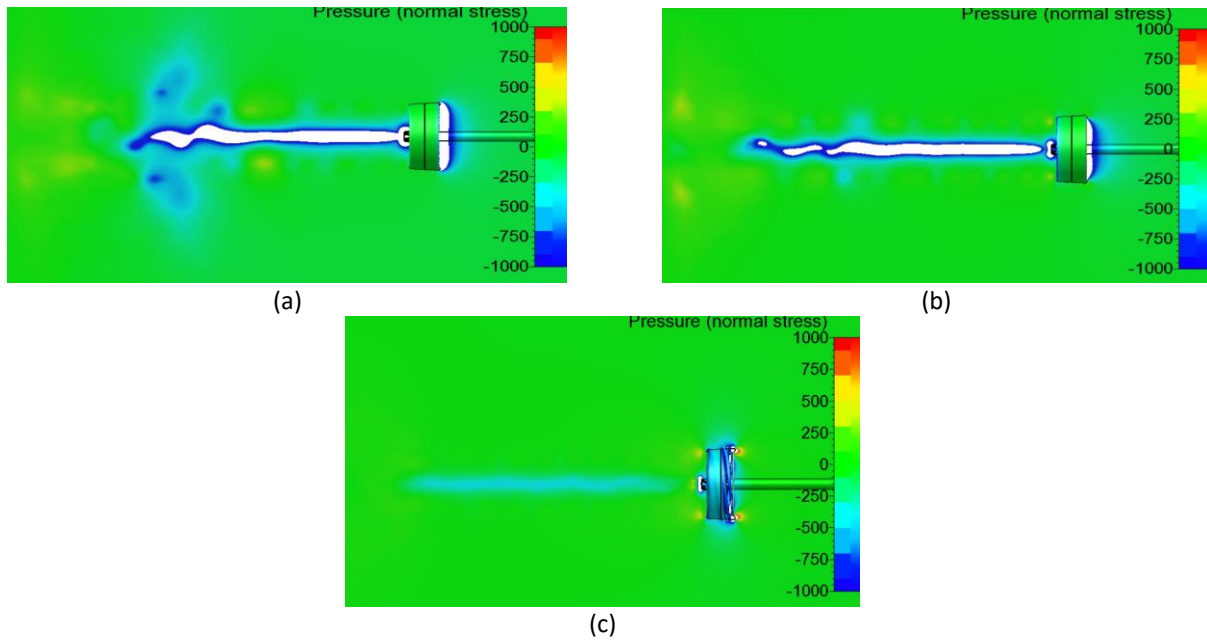

Fig. 29. Visualization of pressure on the Ka4-70 propeller with nozzle 19A and BCF straight (a) Pressure at J= 0.1 (b) Pressure at J= 0.5 (c) Pressure at J= 0.9
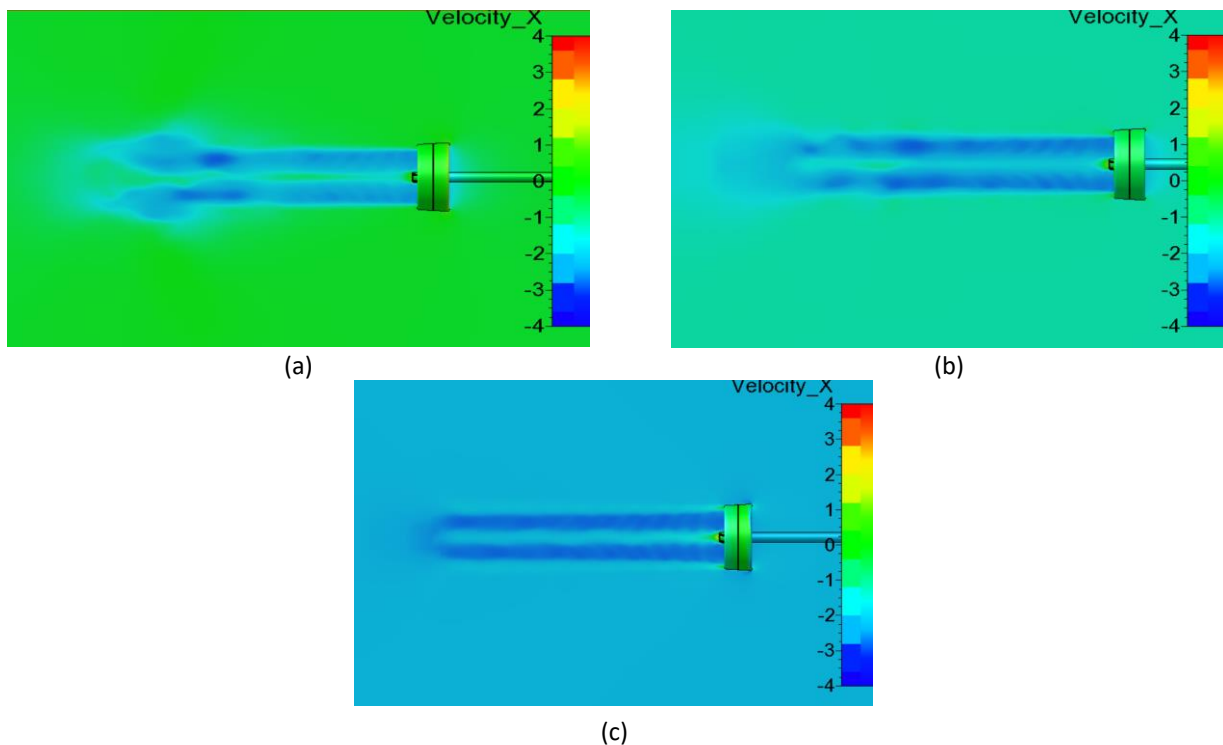

Fig. 30. Visualization of velocity on the propeller Ka4-70 with nozzle 19A and BCF straight (a) Velocity at J= 0.1 (b) Velocity at J= 0.5 (c) Velocity at J= 0.9

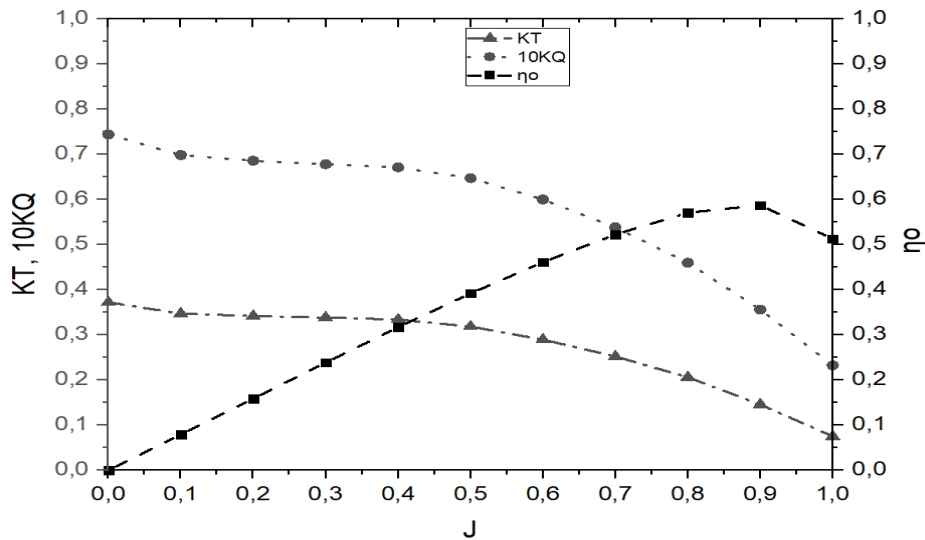The results of Propeller Ka4-70 with nozzle 19A and BCF convergent calculation are shown in Figure 31.

Fig. 31. Open water test diagram of Ka4-70 with nozzle 19A and BCF convergent

The open water test graph of the Ka4-70 Propeller with nozzle 19A and BCF convergent, obtained from CFD simulations presented in Figure 21 shows that at J = 0.1, the value of K_T is 0.347 and decreases to 0.318 at J = 0.5, reaching its lowest point at J = 1.0 with a value of 0.075. A similar trend is observed for the value of $10K_Q$, where it is 0.698 at J = 0.1 and decreases to 0.647 at J = 0.5, reaching its lowest value at J = 1.0 with a value of 0.232. However, the efficiency behaves differently, as the lowest value at J = 0.1 increases at J = 0.5, reaching the peak efficiency of 0.587 at J = 1.0. Therefore, it can be concluded that for the Ka4-70 Propeller with nozzle 19A and BCF convergent, at low speeds, the efficiency is also low but the values of K_T and $10K_Q$ are high. The highest value of η_0 is 0.587 at J = 0.9 [37].

The pressure visualization of the Ka4-70 Propeller with nozzle 19A and convergent Boss Cap Fins reinforces the results of the CFD simulation in Figure 32. The outcomes presented in the graphs demonstrate that at low speeds, J = 0, there is a high K_T value of 0.347; at moderate speeds, J = 0.5, the K_T value is 0.318; while at high speeds, J = 0.9, the K_T value is 0.146. In the region of the convergent boss cap fins, significant pressure occurs at J = 0.1, exceeding 1000 Pa; similarly, at J = 0.5, the pressure is also above 1000 Pa, but the pressure value is lower at J = 0.9, ranging from 250 to 500 Pa. This study highlights that the Ka4-70 Propeller with nozzle 19A and convergent Boss Cap Fins experiences substantial pressure at low speeds, J = 0.1, up to moderate speeds, J = 0.5, indicating a need for a solution to reduce the pressure.

The visualization of the velocity of the Ka4-70 propeller with the nozzle 19A and the convergent BCF (Boss Cap Fins) strengthens the results obtained from the CFD simulation in terms of pressure values. In the boss cap fin, there is significant pressure when J = 0.1, exceeding 1000 Pa, and similarly, when J = 0.5, it remains above 1000 Pa, but the pressure values are lower when J = 0.9, ranging from 250 Pa to 500 Pa. In this study, the Ka4-70 propeller with the 19A nozzle and the convergent BCF experiences high pressure at low speeds (J = 0.1) up to moderate speeds (J = 0.5), thus necessitating a solution to reduce this pressure. The visualization of the velocity of the Ka4-70 propeller with the 19A nozzle and the convergent BCF strengthens the CFD simulation results regarding pressure values. Starting from J = 0.1, the blade section exhibits induced axial velocities ranging from 2 m/s to 3 m/s, while at the boss cap of the propeller, the flow velocity remains between 0 m/s and 1 m/s.

Meanwhile, in the blade section at J = 0.5, the induced axial velocity ranges from 3 m/s to 4 m/s, and in the boss cap of the propeller, there is flow with velocities ranging from 0 m/s to 3 m/s. At J = 0.9, the induced axial velocity in the blade section is 3 m/s to 4 m/s, although there is an increase in flow velocity at the boss cap of the propeller, ranging from 0 m/s to 3 m/s. In conclusion, for the Ka4-70 propeller with the 19A nozzle and the convergent BCF, it can be observed that as the value of J (advanced coefficient) increases, the flow velocity at both the boss cap and the propeller blade increases [22].
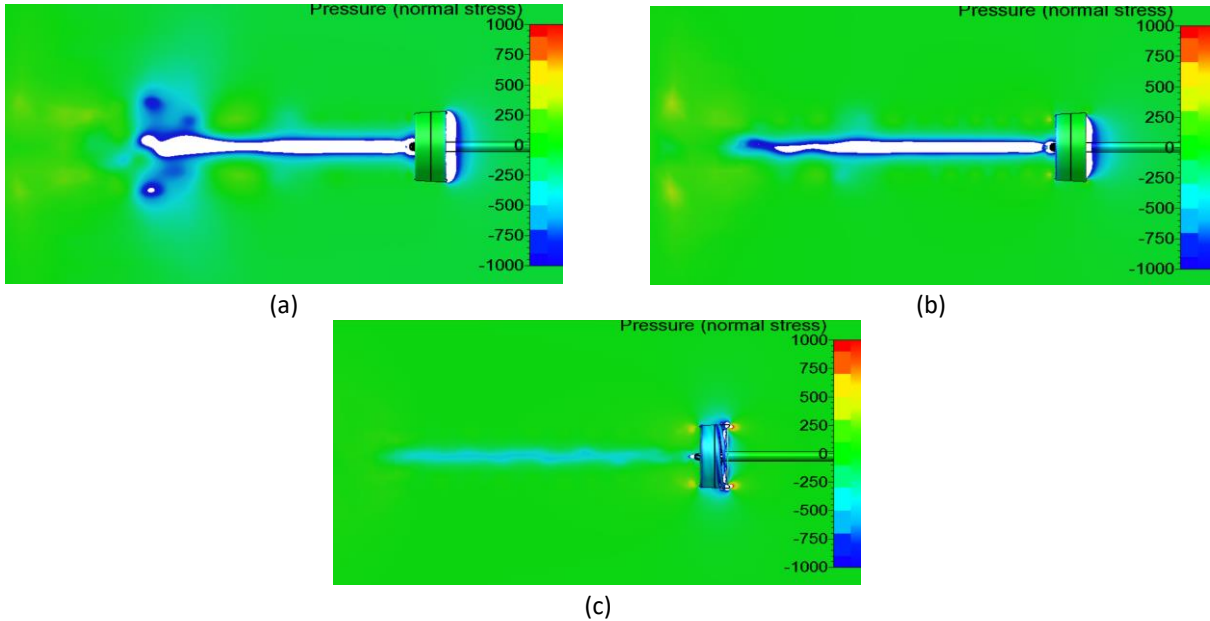

(a)

(b)

(c)

Fig. 32. Visualization of pressure on the Ka4-70 propeller with nozzle 19A and BCF convergent (a) Pressure at J= 0.1(b) Pressure at J= 0.5 (c) Pressure at J= 0.9
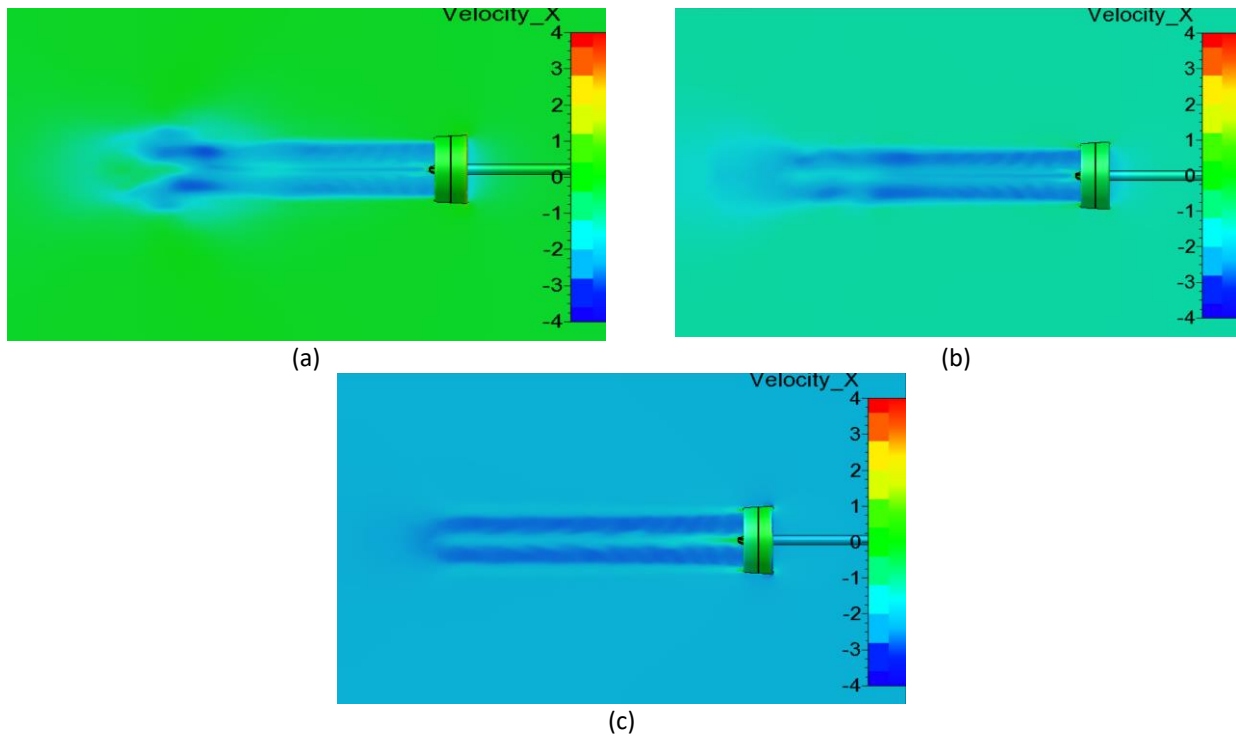

(a)

(b)

(c)

Fig. 33. Visualization of velocity on the propeller Ka4-70 with nozzle 19A and BCF convergent (a) Velocity at J= 0.1 (b) Velocity at J= 0.5 (c) Velocity at J= 0.9

The results of Propeller Ka4-70 with nozzle 19A and BCF divergent calculation are shown in Figure 34.
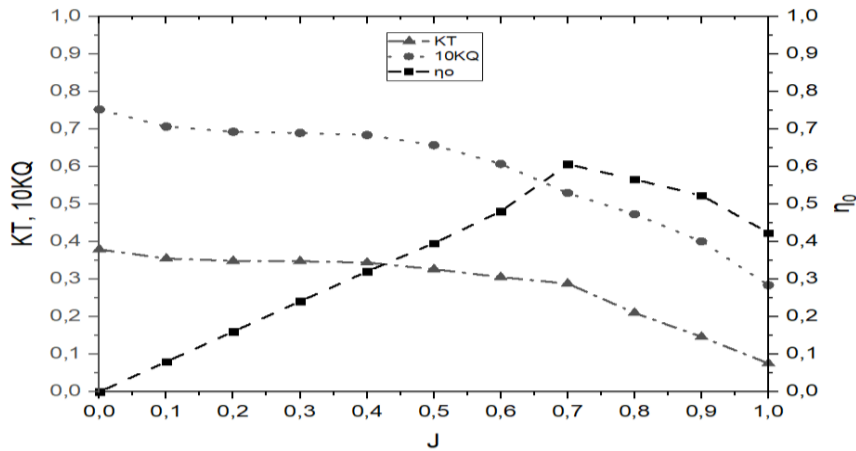

Fig. 34. Open water test diagram of Ka4-70 nozzle 19A and BCF divergent

The graph shown in Figure 34 of the open water test for Propeller Ka4-70 with nozzle 19A and BCF divergent is obtained from CFD simulations. At J = 0.1, the K_T value is 0.355, which decreases to 0.337 at J = 0.5 and reaches its lowest point at J = 1.0 with a value of 0.076. Similarly, at J = 0.1, the $10K_Q$ value is 0.706, which decreases to 0.657 at J = 0.5 and reaches its lowest point at J = 1.0 with a value of 0.284 [38]. However, the efficiency value shows the opposite trend. The lowest efficiency value is observed at J = 0.1, which increases to 0.396 at J = 0.5 and reaches its peak value of 0.606 at J = 0.7. In conclusion, for Propeller Ka4-70 with nozzle 19A and BCF divergent, at low speeds, the efficiency value is low while the K_T and $10K_Q$ values are high. On the other hand, the highest efficiency value of 0.606 is achieved at J = 0.7 [39].
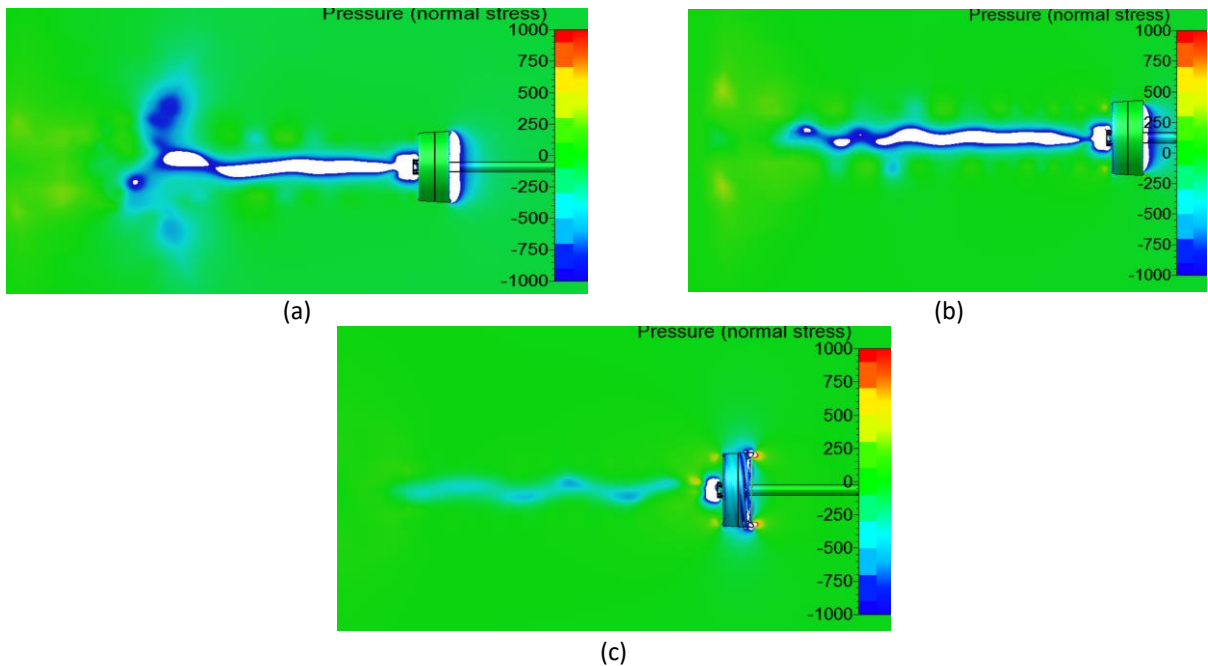

(a)

(b)

(c)

Fig. 35. Visualization of pressure propeller Ka4-70 with nozzle 19A and BCF divergent (a) Pressure at J= 0.1 (b) Pressure at J= 0.5 (c) Pressure at J= 0.7

The CFD simulation of Propeller Ka4-70 with nozzle and BCF divergent shows that the highest efficiency value (η_0) is 0.521 for Propeller Ka4-70 with nozzle 19A and BCF divergent. The pressure distribution on Propeller Ka4-70 with nozzle 19A and BCF divergent reveals high pressure in the boss cap fins region when J = 0.1, exceeding 1000 Pa. Similarly, at J = 0.5, the pressure is also above 1000 Pa [40]. However, at J = 0.7, the pressure values are smaller, ranging from 250 Pa to 750 Pa. In this study, Propeller Ka4-70 with nozzle 19A and BCF divergent experiences high pressure at low speeds J = 0.1 up to moderate speeds J = 0.5 [40].
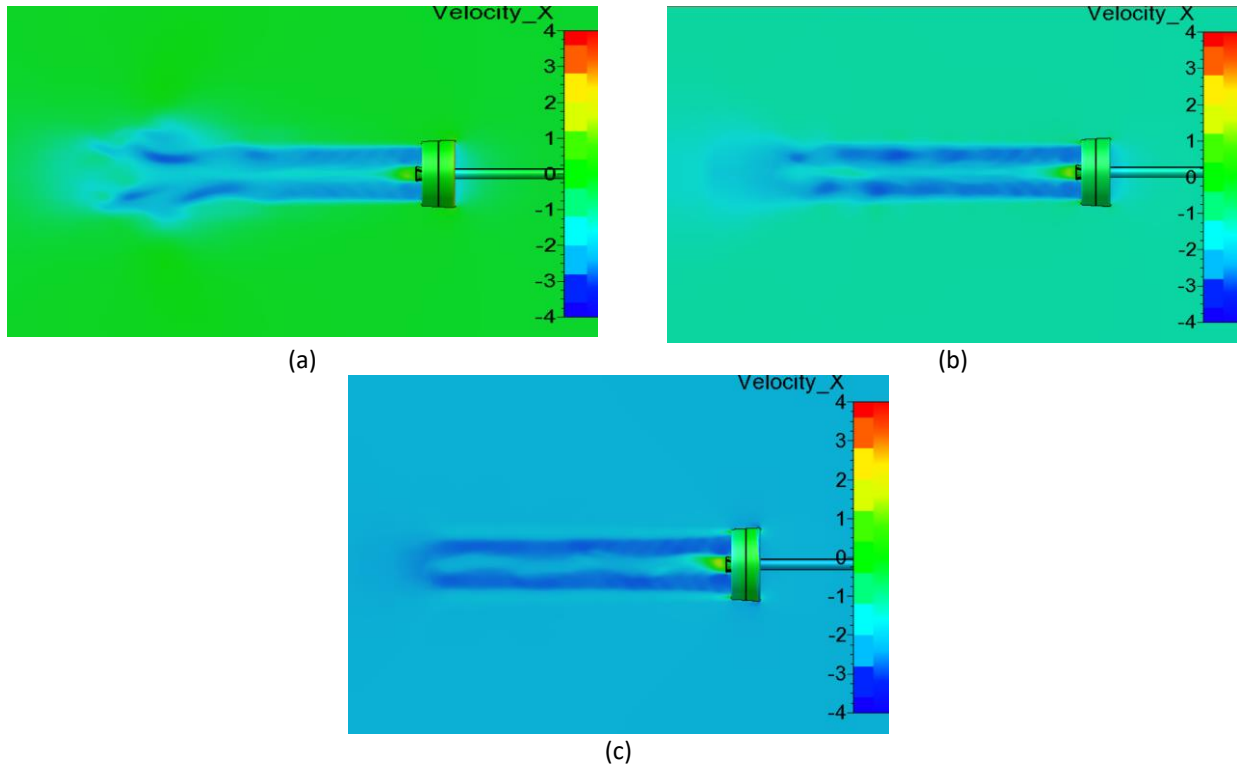

Fig. 36. Visualization of velocity on the propeller Ka4-70 with 19A nozzle and BCF divergent (a) Velocity at J= 0.1 (b) Velocity at J= 0.5 (c) Velocity at J= 0.9

The visualization of the velocity of the Ka4-70 propeller with the nozzle 19A and the BCF (Boss Cap Fins) divergent strengthens the results obtained from the CFD simulation in terms of pressure values. In the boss cap fin, there is significant pressure when J = 0.1, exceeding 1000 Pa, and similarly, when J = 0.5, it remains above 1000 Pa, but the pressure values are lower when J = 0.9, ranging from 250 Pa to 500 Pa. In this study, the Ka4-70 propeller with the nozzle 19A and the BCF divergent experiences high pressure at low speeds (J = 0.1) up to moderate speeds (J = 0.5), thus necessitating a solution to reduce this pressure. The visualization of the velocity of the Ka4-70 propeller with the nozzle 19A and the divergent BCF strengthens the CFD simulation results regarding pressure values. Starting from J = 0.1, the blade section exhibits induced axial velocities ranging from 2 m/s to 4 m/s, while at the boss cap of the propeller, the flow velocity remains between 0 m/s and 2 m/s. Meanwhile, in the blade section at J = 0.5, the induced axial velocity ranges from 3 m/s to 4 m/s, and in the boss cap of the propeller, there is flow with velocities ranging from 0 m/s to 2 m/s. At J = 0.9, the induced axial velocity in the blade section is 3 m/s to 4 m/s, although there is an increase in flow velocity at the boss cap of the propeller, ranging from 0 m/s to 2 m/s [39]. In conclusion, for the Ka4-70 propeller with the nozzle 19A and the BCF divergent, it can be observed that as the value of J (advanced coefficient) increases, the flow velocity at the propeller blade increases, while the flow velocity at the boss cap remains the same [41].

5. Conclusion

Reynolds Averaged Navier Stokes Equation (RANSE) was employed in this investigation of technical aspects and upcoming hurdles in energy-efficient propeller technology. Propeller designs for B4-70 and Ka4-70 were developed to investigate the impact of Energy-Saving Devices (ESD) on propeller efficiency. The CFD simulation results for both B4-70 and Ka4-70 propellers, utilizing a nozzle 19A with added boss cap fins, revealed several noteworthy phenomena. Firstly, for the B4-70 propeller, the thrust coefficient (K_T) exhibited an average increase of 5% to 6% when transitioning from J = 0.6 to J = 0.8, while the torque coefficient ($10K_Q$) increased by 3% to 4%. The propeller efficiency (η_0) at J = 0.6 to J = 0.8 also showed an increase of 1% to 2%. Secondly, concerning the Ka4-70 propeller, the K_T values saw an average increase of 4% to 20% when transitioning from J = 0.6 to J = 0.8, and the $10K_Q$ values increased by 5% to 16%. Furthermore, the propeller efficiency (η_0) at J = 0.6 to J = 0.8 increased by 2% to 10%. These findings clearly demonstrate that the use of an ESD, such as the nozzle 19A with added boss cap fins, enhances the propulsion performance of the ship. It is evident that the CFD approach remains suitable and reliable for overall simulations.

References
[1] United nations Conference on Trade and Development (UNCTAD). 2021. Review of Maritime Report 2021. New York: United nations Conference on Trade and Development (UNCTAD).
[2] Jasper, F., and H. Shinichi. "Fourth IMO Greenhouse Gas Study 2020." *International Maritime Organisation (IMO), London, UK* (2020).
[3] DNV. 2021. "Maritime Forecast To 2050 - Energy Transition Outlook 2021." Høviky.
[4] International Maritime Organization. 2021. "IMO's Work to Cut GHG Emissions from Ships."
[5] International Maritime Organization. 2021. "Fourth IMO GHG Study 2020 Full Report."
[6] Kawamura, Takafumi, Kazuyuki Ouchi, and Takeo Nojiri. "Model and full scale CFD analysis of propeller boss cap fins (PBCF)." *Journal of marine science and technology* 17 (2012): 469-480.
[7] Seo, Jeonghwa, Seung-Jae Lee, Bumwoo Han, and Shin Hyung Rhee. "Influence of design parameter variations for propeller-boss-cap-fins on hub vortex reduction." *Journal of Ship Research* 60, no. 04 (2016): 203-218. https://doi.org/10.5957/JOSR.60.4.160003
[8] Adietya, Berlian Arswendo, I. Ketut Aria Pria Utama, and Wasis Dwi Aryawan. "CFD Analysis into the Effect of using Propeller Boss Cap Fins (PBCF) on Open and Ducted Propellers, Case Study with Propeller B-Series and Kaplan-Series." *CFD Letters* 14, no. 4 (2022): 32-42. https://doi.org/10.37934/cfdl.14.4.3242
[9] Ridwan, M., B. A. Adietya, and D. Chrismianto. "Stability analysis of trawls type traditional fishing boat with modification of eco-friendly fishing-gear on the north coast of Central Java." In *IOP Conference Series: Materials Science and Engineering*, vol. 403, no. 1, p. 012052. IOP Publishing, 2018. https://doi.org/10.1088/1757-899X/403/1/012052
[10] Kiryanto, Mohammad Ridwan, Berlian Arswendo Adietya, Deddy Chrismianto, and Sri Hartanto Aji Sasongko. "Stability and total resistance analysis of catamaran fishing boat for Java North Sea area with hullform model and fishing gear variation." *International Journal of Mechanical Engineering and Technology (IJMET) Vol* 10, no. 01 (2019): 1291-1302.
[11] Chrismianto, Deddy, Ahmad Fauzan Zakki, Berlian Arswendo, and Insanu Abdilla Cendikia Abar. "Comparison of Propeller Type B-Series and Au-Outline Gawn Series for Improving on Submarine Propulsion Performance using CFD." *International Journal of Advanced Research in Engineering and Technology* 10, no. 2 (2019).
[12] Adietya, Berlian Arswendo, Aulia Windyandari, and Ahmad Fauzan Zakki. "The Study on Stability and Seakeeping Characteristics of the Glass Bottom Boat Trimaran in Karimunjawa Island." In *IOP Conference Series: Earth and Environmental Science*, vol. 135, no. 1, p. 012007. IOP Publishing, 2018. https://doi.org/10.1088/1755-1315/135/1/012007

[13] Ariana, I. Made, Riyan Bagus Prihandanu, Dhimas Widhi Handani, and A. A. B. Dinariyana. "Investigation of the Effects of the Pre-Duct in a Ship on Propeller–Hull Interactions Using the CFD Method." *CFD Letters* 15, no. 4 (2023): 17-30. https://doi.org/10.37934/cfdl.15.4.1730

[14] Organızatıon, Internatıonal Marıtıme. "Guidelines for voluntary use of the ship energy efficiency operational indicator (EEOI)." *London: IMO* (2009).

[15] Mewis, Friedrich. "A novel power-saving device for full-form vessels." In *First International Symposium on Marine Propulsors, SMP*, vol. 9. 2009.

[16] Celik, Ishmail B., Urmila Ghia, Patrick J. Roache, and Christopher J. Freitas. "Procedure for estimation and reporting of uncertainty due to discretization in CFD applications." *Journal of fluids Engineering-Transactions of the ASME* 130, no. 7 (2008). https://doi.org/10.1115/1.2960953

[17] Darsono, Febri Budi, Rahmad Doni Widodo, and Akhmad Nurdin. "Analysis Of the Effect of Flow Rate and Speed on Four Blade Tubular Water Bulb-Turbine Efficiency Using Numerical Flow Simulation." *Journal of Advanced Research in Fluid Mechanics and Thermal Sciences* 90, no. 2 (2021): 1-8. https://doi.org/10.37934/arfmts.90.2.18

[18] Niknahad, Ali. "Numerical study and comparison of turbulent parameters of simple, triangular, and circular vortex generators equipped airfoil model." *Journal of Advanced Research in Numerical Heat Transfer* 8, no. 1 (2022): 1-18.

[19] Wallin, Stefan. *Engineering turbulence modelling for CFD with focus on explicit algebraic Reynolds stress models*. Stockholm, Sweden: Royal Institute of Technology, Department of Mechanics, 2000.

[20] Xing, L. H., G. B. Huang, and Min Yan. "Numerical Simulation of 3D Density Flow by an Improved EASM Model." *Procedia Environmental Sciences* 10 (2011): 753-758. https://doi.org/10.1016/j.proenv.2011.09.122

[21] Matsuda, Satoshi, and Tokihiro Katsui. "Hydrodynamic Forces and Wake Distribution of Various Ship Shapes Calculated Using a Reynolds Stress Model." *Journal of Marine Science and Engineering* 10, no. 6 (2022): 777. https://doi.org/10.3390/jmse10060777

[22] Adietya, B. A., W. D. Aryawan, and I. K. A. P. Utama. "A study into the effect tip clearance on the performance of b-series and kaplan-series ducted propellers." In *IOP Conference Series: Earth and Environmental Science*, vol. 1166, no. 1, p. 012038. IOP Publishing, 2023. https://doi.org/10.1088/1755-1315/1166/1/012038

[23] Mizzi, Kurt, Yigit Kemal Demirel, Charlotte Banks, Osman Turan, Panagiotis Kaklis, and Mehmet Atlar. "Design optimisation of Propeller Boss Cap Fins for enhanced propeller performance." *Applied Ocean Research* 62 (2017): 210-222. https://doi.org/10.1016/j.apor.2016.12.006

[24] Bahatmaka, Aldias, Aditya Rio Prabowo, and Dong-Joon Kim. "Effect of Nozzle Performance on the Ducted Propeller: A Benchmark-Simulation Study using OpenFOAM." *Transportation Research Procedia* 55 (2021): 645-652. https://doi.org/10.1016/j.trpro.2021.07.031

[25] Gatski, Thomas B., and Charles G. Speziale. "On explicit algebraic stress models for complex turbulent flows." *Journal of fluid Mechanics* 254 (1993): 59-78. https://doi.org/10.1017/S0022112093002034

[26] Gao, Qiuxin, Wei Jin, and Dracos Vassalos. "The calculations of propeller induced velocity by RANS and momentum theory." *Journal of Marine Science and Application* 11, no. 2 (2012): 164-168. https://doi.org/10.1007/s11804-012-1118-1

[27] Andersson, Bengt, Ronnie Andersson, Love Håkansson, Mikael Mortensen, Rahman Sudiyo, and Berend Van Wachem. *Computational fluid dynamics for engineers*. Cambridge university press, 2011.

[28] Gaggero, Stefano, Juan Gonzalez-Adalid, and Mariano Perez Sobrino. "Design of contracted and tip loaded propellers by using boundary element methods and optimization algorithms." *Applied Ocean Research* 55 (2016): 102-129. https://doi.org/10.1016/j.apor.2015.12.004

[29] Gaggero, Stefano, Juan Gonzalez-Adalid, and Mariano Perez Sobrino. 2016. "Design of Contracted and Tip Loaded Propellers by Using Boundary Element Methods and Optimization Algorithms." Applied Ocean Research 55 (February): 102–29. https://doi.org/10.1016/j.apor.2015.12.004

[30] Bhattacharyya, Anirban, Vladimir Krasilnikov, and Sverre Steen. "A CFD-based scaling approach for ducted propellers." *Ocean engineering* 123 (2016): 116-130. https://doi.org/10.1016/j.oceaneng.2016.06.011

[31] Gaggero, Stefano, Diego Villa, Giorgio Tani, Michele Viviani, and Daniele Bertetta. "Design of ducted propeller nozzles through a RANSE-based optimization approach." *Ocean Engineering* 145 (2017): 444-463. https://doi.org/10.1016/j.oceaneng.2017.09.037

[32] Andersson, Jennie, Arash Eslamdoost, Marko Vikström, and Rickard E. Bensow. "Energy balance analysis of model-scale vessel with open and ducted propeller configuration." *Ocean Engineering* 167 (2018): 369-379. https://doi.org/10.1016/j.oceaneng.2018.08.047

[33] Bontempo, R., and M. Manna. "Performance analysis of ducted marine propellers. Part II–Accelerating duct." *Applied Ocean Research* 75 (2018): 153-164. https://doi.org/10.1016/j.apor.2018.03.005

[34] Trimulyono, Andi, A. B. Jatmiko, I. P. Mulyatno, and H. Yudo. "The effect of propeller cap angle and fin size of PBCF on propeller performance." In *IOP Conference Series: Earth and Environmental Science*, vol. 972, no. 1, p. 012045. IOP Publishing, 2022. https://doi.org/10.1088/1755-1315/972/1/012045

[35] Bosschers, Johan, Chris Willemsen, Adam Peddle, and Douwe Rijpkema. "Analysis of ducted propellers by combining potential flow and RANS methods." In *Fourth International Symposium on Marine Propulsors*, pp. 639-648. 2015.

[36] Haimov, Henri, Jorge Vicario, and Javier Del Corral. "RANSE code application for ducted and endplate propellers in open water." In *Proceedings of the Second International Symposium on Marine Propulsors*, pp. 1-9. 2011.

[37] Gaggero, Stefano, Diego Villa, Giorgio Tani, and Michele Viviani. "Propeller nozzles design using viscous codes and optimization algorithms." In *MARINE VI: proceedings of the VI International Conference on Computational Methods in Marine Engineering*, pp. 234-255. CIMNE, 2017.

[38] Zhang, Qin, and Rajeev K. Jaiman. "Numerical analysis on the wake dynamics of a ducted propeller." *Ocean Engineering* 171 (2019): 202-224. https://doi.org/10.1016/j.oceaneng.2018.10.031

[39] Nojiri, Takeo, Norio Ishii, and Hisashi Kai. 2011. "Energy Saving Technology of PBCF (Propeller Boss Cap Fins) and Its Evolution." *Journal of The Japan Institute of Marine Engineering* 46 (3): 350–358. https://doi.org/10.5988/jime.46.350

[40] Adietya, Berlian Arswendo, I. Ketut Aria Pria Utama, Wasis Dwi Aryawan, Mochammad Nasir, Mahendra Indiaryanto, Nurwidhi Asrowibowo, and Rizqi Dian Permana. "Numerical and Experimental Investigations into the Characteristics of Wageningen B4-70 Series of Propeller with Boss Cap Fins." *CFD Letters* 15, no. 10 (2023): 152-169. https://doi.org/10.37934/cfdl.15.10.152169

[41] Tani, Giorgio, Diego Villa, Stefano Gaggero, Michele Viviani, Pierluigi Ausonio, Piero Travi, Giovanni Bizzarri, and Francesco Serra. "Experimental investigation of pressure pulses and radiated noise for two alternative designs of the propeller of a high-speed craft." *Ocean Engineering* 132 (2017): 45-69. https://doi.org/10.1016/j.oceaneng.2017.01.015